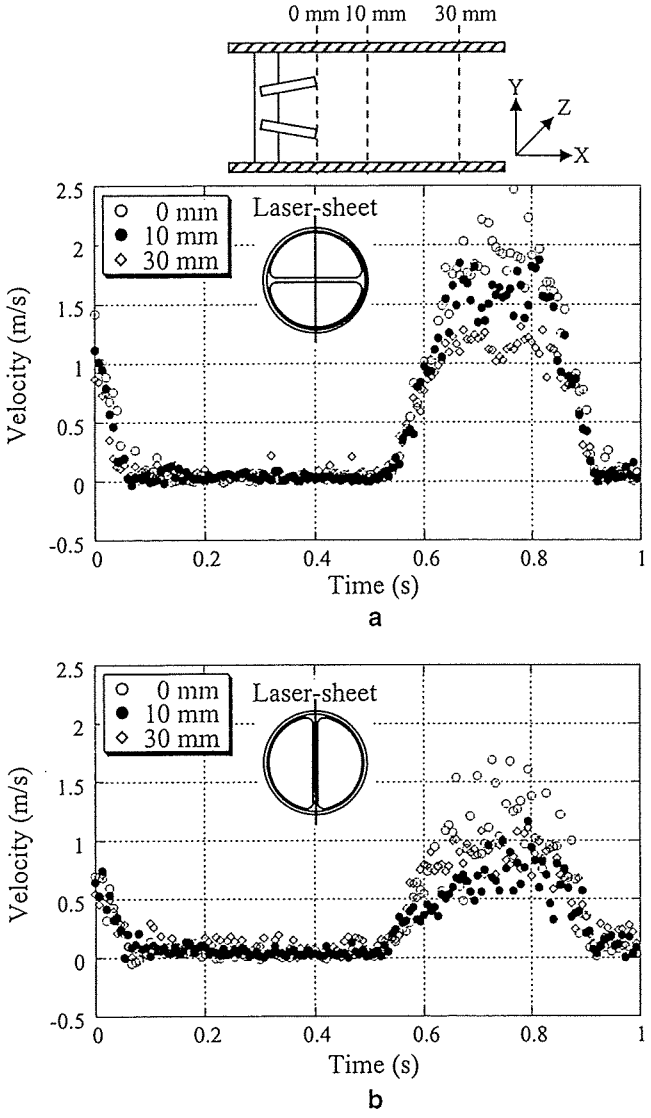

Fig. 9. The maximum flow velocity of the ATS valve according to the distance from the opened leaflet: a X-Y plane, b X-Z plane

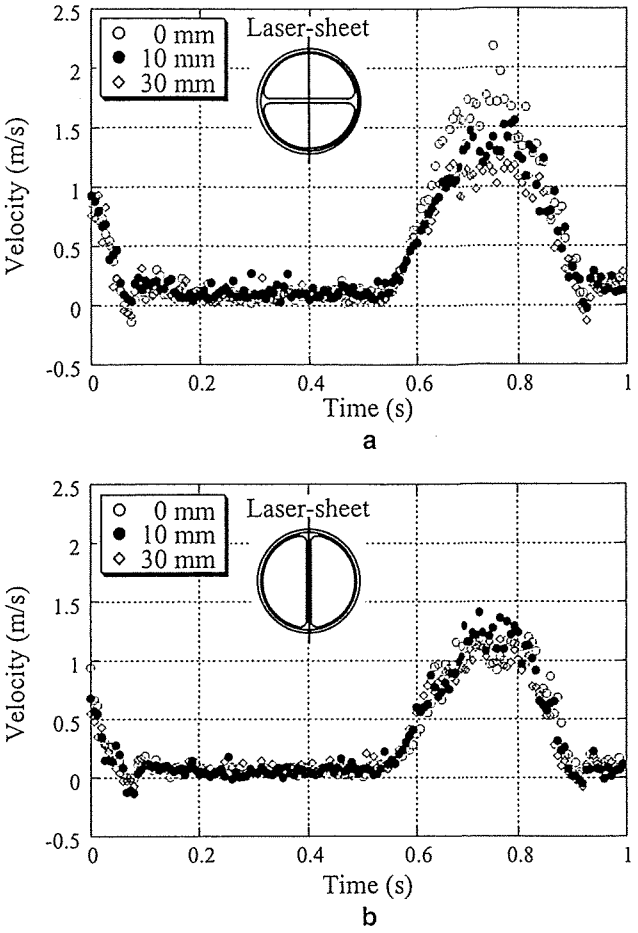

Fig. 10. The maximum flow velocity of the St. Jude valve according to the distance from the opened leaflet: a X-Y plane, b X-Z plane

0.12 m/s in the X-Y plane (Fig. 11a). There was no significant difference between the values in the X-Z plane and those in the X-Y plane. The maximum velocity range of the Sorin Bicarbon valve in the X-Y plane was less than those of the other two valves. There was no significant different in the maximum velocity during the diastolic phase among the three kinds of bileaflet valves (Figs. 9–11).

Discussion

In the present study, we used the PIV method to visualize flow downstream of the outlet valve in a PVAD. Other groups have visualized the effect of flow on the sinus cavity[8–10,21] and examined the condition of the implantable MHV in a natural heart.[12,22] Still other groups have visualized the flow of a mechanical heart using the simple chamber experimental system.[15,16] The flow visualization of a mechanical heart might differ depending on the experimental system and driving conditions. In the present study, we visualized the flow of a MHV in an artificial heart in which there is no sinus cavity and the boundary conditions differ from those of a natural heart. Moreover, the flow velocity pattern varies according to the leaflet geometry of the bileaflet valve (Figs. 6–8). The leaflet geometry of the ATS and St. Jude valves was flat, which means that there may be turbulent flow across the leaflet during the systole phase. We think that a strong turbulent flow might be related to the valve opening motion. In the future, we will investigate the relationship between the turbulent flow and the valve opening motion. In contrast, the curved-leaflet geometry of the Sorin Bicarbon valve minimized flow disturbances compared to the situation with flat-leaflet valves,[10] and this might reduce the turbulent flow. In this study, we investigated the flow velocity at the central location of the X-Z and X-Y planes. As shown in Fig. 11, the flow velocity of the Sorin Bicarbon valve in the X-Z plane was higher than that of the other valves. The curved leaflets of the Sorin Bicarbon valve provide a wider opening area of the central orifice when the valve is fully opened. This increased central orifice area is the direct reason for the increase in velocity. Therefore, the flow velocity in the X-Y plane was lower

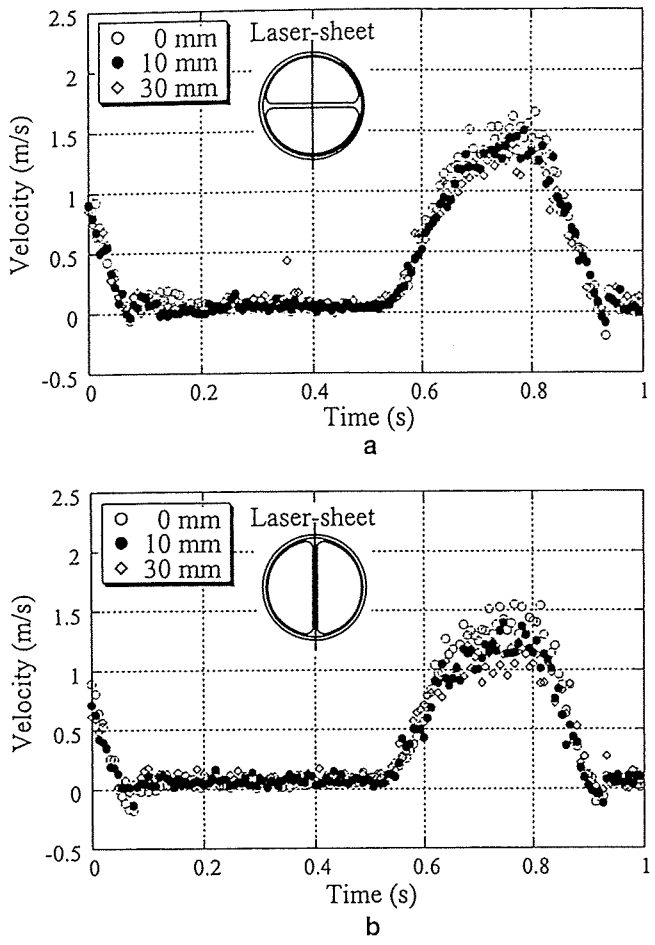

Fig. 11. The maximum flow velocity of the Sorin Bicarbon valve according to the distance from the opened leaflet: a X-Y plane, b X-Z plane

than that of the ATS and St. Jude valves. Grigioni et al. investigated the influence of leaflet curvature on the flow field in the St. Jude and Sorin Bicarbon valves,[10] reporting that the curved leaflet exhibits reduced turbulent intensities compared with those of the flat leaflet, which is seemingly consistent with the present results judging from the velocity field. Even though the three types of valves have identical sewing ring diameters, the orifice diameters are different, with that of the Sorin Bicarbon valve being larger than those of the other two valves (Table 1). This means that if the three valves have the same bypass flow, the mean flow velocity of the Sorin Bicarbon valve will be 6.5% and 5.3% less than that of the St. Jude valve and the ATS valve, respectively. Because the driving conditions of our PVAD differ from those of the natural heart, a higher flow velocity occurs during the systole phase.

The opening angle of the valve is an important feature of its geometry. In the present study, we estimated the opening point of the outlet valve using the bypass flow waves (Fig. 5). There were no differences in the valve opening points. However, the bypass flow of the ATS valve during the early systole phase was higher that that of the other valves. This is consistent with the results for the flow velocity vectors downstream of the bileaflet valves (Figs. 6–8). The closing volume of the St. Jude valve was larger than that of the other valves.

The density of blood is approximately 1.06 g/cm^3, which is much less than the density of the present working fluid. The present results are therefore not appropriate for in vivo testing. However, to investigate the optimal bileaflet valve for our PVAD, we first investigated the downstream flow velocity of three bileaflet valves with different geometries. In order to accurately measure the flow velocity inside a model pump made of acrylic resin, it is more important to use a fluid with the same refractive index as acrylic resin than to use a fluid with the same density as blood. However, fluid density is an important factor when investigating the Reynolds shear stress as a cause of hemolysis. In future studies, we will examine the Reynolds shear stress using a working fluid with a fluid density of 1.06 g/cm^3. Moreover, in this study, as shown in the visualization of velocity vectors (Figs. 6–8), the effect of the seeding methods on the velocity vector could not found. In this study, we measured the flow visualization during three cycles only. However, in order to minimize the flow velocity inside of the model pump and near the leaflet, the model pump was run using the full-filling and full-ejection condition under the low heart rate of 70 bpm. There were no significant differences in the flow pattern among the cycles, and the results have a small standard deviation.

When developing a VAD, thrombus formation inside the blood pump is also important. In a previous study, we compared the flow pattern inside a blood pump with a monoleaflet (Medtronic Hall valve) valve with one with a bileaflet valve (Sorin Bicarbon valve). We reported that there were no significant differences between the valves in the average flow velocity at the diaphragm–housing junction.[23] This means that a bileaflet valve might be applicable to our PVAD from the point of view of the washout effect inside the blood pump. In the present study, we did not investigate the hemolysis caused by the three kinds of bileaflet valves during the systolic phase. In the future, we will estimate the thrombus formation at the diaphragm–housing junction using in vivo testing.

Conclusions

In the present study, we visualized the flow downstream from bileaflet valves using the PIV method, and found a higher flow velocity near the leaflet during the systole phase. The Sorin Bicarbon curved-leaflet valve creates a large central flow, which decreases the flow velocity and reduces turbulence. Although the tested bileaflet valves are very similar in design, the pattern of the flow velocity differs according to the geometry of the leaflet. The leaflet geometry was therefore determined to be an important parameter when selecting a MHV for use in our PVAD.

Acknowledgments This work was supported by the Program for the Promotion of Fundamental Studies in Health Science of the National Institute of Biomedical Innovation (NIBIO).

References

1. Stevenson LW, Kormos RL. Mechanical cardiac support 2000: current applications and future trial design. J Heart Lung Transplant 2001;20:1–38
2. Nakata M, Masuzawa T, Tatsumi E, Taenaka Y, Nishimura T, Tsukiya T, Takano H, Tsuchimoto K, Ohba K. Characterization and optimization of the flow pattern inside a diaphragm blood pump based on flow visualization techniques. ASAIO J 1998;44: M714–M718
3. Kafesjian R, Howanec M, Ward GD, Diep L, Wagstaff LS, Rhee R. Cavitation damage of pyrolytic carbon in mechanical heart valves. J Heart Valve Dis 1994;3(Suppl I):S2–S7
4. Wu C, Liu JS, Hwang NHC, Lin YKM. Statistical correlation between transient pressure drop and cavitation at closure of a mechanical heart valve. ASAIO J 2005;51:11–16
5. Lukic B, Zapanta CM, Griffith KA, Weiss WJ. Effect of the diastolic and systolic duration on valve cavitation in a pediatric pulsatile ventricular assist device. ASAIO J 2005;51:546–550
6. Sohn K, Manning KB, Fontaine AA, Tarbell JM, Deutsch S. Acoustic and visual characteristics of cavitation induced by mechanical heart valves. J Heart Valve Dis 2005;14:551–558
7. Leverett LB, Hellums JD, Alfrey CP, Lynch EC. Red blood cell damage by shear stress. Biophys J 1972;12:257–273
8. Liu JS, Lu PC, Lo CW, Lai HC, Hwang NHC. An experimental study of steady flow patterns of a new trileaflet mechanical aortic valve. ASAIO J 2005;51:336–341
9. Lim WL, Chew YT, Chew TC, Low HT. Pulsatile flow studies of a porcine bioprosthetic aortic valve in vitro: PIV measurements and shear-induced blood damage. J Biomech 2001;34:1417–1427
10. Grigioni M, Daniele C, D'Avenio G, Barbaro V. The influence of the leaflets' curvature on the flow field in two bileaflet prosthetic heart valves. J Biomech 2001;34:613–621
11. Goubergrits L, Affeld K. Numerical estimation of blood damage in artificial organs. Artif Organs 2004;28:499–507
12. Akutsu T, Saito J. Dynamic particle image velocimetry flow analysis of the flow field immediately downstream of bileaflet mechanical mitral prostheses. J Artif Organs 2006;9:165–178
13. Castellini P, Pinotti M, Scalise L. Particle image velocimetry for flow analysis in longitudinal planes across a mechanical artificial heart valve. Artif Organs 2004;28:507–513
14. Subramanian A, Mu H, Kadambi JR, Wernet MP, Brendzel AM, Harasaki H. Particle image velocimetry investigation of intravalvular flow fields of a bileaflet mechanical heart valve in a pulsatile flow. J Heart Valve Dis 2000;9(5):721–731
15. Manning KB, Kini V, Fontaine AA, Deutsch S, Tarbell JM. Regurgitant flow field characteristics of the St. Jude bileaflet mechanical heart valve under physiologic pulsatile flow using particle image velocimetry. Artif Organs 2003;27(9):840–846
16. Kini V, Bachmann C, Fontaine A, Deutsch S, Tarbell JM. Integrating particle image velocimetry and laser Doppler velocimetry measurements of the regurgitant flow field past mechanical heart valves. Artif Organs 2001;25:136–145
17. Heise M, Schmidt S, Krüger U, Rückert R, Rösler S, Neuhaus P, Settmacher U. Flow pattern and shear stress distribution of distal end-to-side anastomoses. A comparison of the instantaneous velocity fields obtained by particle image velocimetry. J Biomech 2004;37:1043–1051
18. Lee HS, Tsukiya T, Homma A, Kamimura T, Takewa Y, Tatsumi E, Taenaka Y, Takano H, Kitamura S. Observation of cavitation bubbles in monoleaflet mechanical heart valves. J Artif Organs 2004;7:121–127
19. Lee HS, Taenaka Y, Kitamura S. Mechanisms of mechanical heart valve cavitation in an electrohydraulic total artificial heart. ASAIO J 2005;51:208–213
20. Akagawa E, Lee HS, Tatsumi E, Homma A, Tsukiya T, Katagiri N, Kakuta Y, Nishinaka T, Mizuno T, Ota K, Kansaku R, Taenaka Y. Effects of mechanical valve orifice direction on flow pattern in a ventricular assist device. J Artif Organs 2007;10:85–91
21. Medart D, Schmitz C, Rau G, Reul H. Design and in vitro performance of a novel bileaflet mechanical heart valve prosthesis. Int J Artif Organs 2005;28:256–263
22. Lu PC, Liu JS, Huang RH, Lo CW, Lai HC, Hwang NHC. The closing behavior of mechanical heart valve prostheses. ASAIO J 2004;50:294–300
23. Akagawa E, Lee HS, Tatsumi E, Homma A, Tsukiya T, Taenaka Y. Effects of mechanism for mechanical heart valve on flow behavior inside the pulsatile blood pump. ASAIO J 2008;54(2):16A

Experimental Study on the Reynolds and Viscous Shear Stress of Bileaflet Mechanical Heart Valves in a Pneumatic Ventricular Assist Device

Hwansung Lee, Eisuke Tatsumi, and Yoshiyuki Taenaka

Our group is currently developing a pneumatic ventricular assist device (PVAD). In general, the major causes of hemolysis in a pulsatile VAD are cavitation, and Reynolds shear stress (RSS) in the mechanical heart valve (MHV). In a previous study, we investigated MHV cavitation. To select the optimal bileaflet valve for our PVAD, in the current study, we investigated RSS and viscous shear stress (VSS) downstream of three different types of commercial bileaflet valves by means of 2D particle image velocimetry (PIV). To carry out flow visualization inside the blood pump and near the valve, we designed a model pump with the same configuration as that of our PVAD. Three types of bileaflet valves (i.e., the ATS valve, the St. Jude valve, and the Sorin Bicarbon valve) were mounted at the aortic position of the model pump, and flow was visualized according to the PIV method. The maximum flow velocity and RSS of the Sorin Bicarbon valve were lower than those of the other two bileaflet valves. The maximum VSS was only 1% of the maximum RSS. Thus, the effect of VSS on blood cell trauma was neglected. The Sorin Bicarbon valve exhibited relatively low levels of RSS, and was therefore considered to be the best valve for our PVAD among the three valves tested. *ASAIO Journal* 2009; 55:348–354.

The use of a mechanical circulatory support device such as a ventricular assist device (VAD) has become standard therapy as a bridge to transplantation. In recent years, the most frequently used devices have been the pulsatile VAD, the Berlin Heart VAD, the Thoratec VAD system (Pierce-Donachy), the Novacor II, the WorldHeart HeartSaverVAD, the Abiomed Biventricular Support (BVS) 5000, and the Arrow LionHeart VAD.[1] The Berlin Heart VAD uses a tilting disc and a polyurethane velum valve. The Thoratec VAD system (Pierce-Donachy) and Arrow LionHeart VAD each use a tilting disc valve, and the Novacor II uses a bovine pericardial tissue valve. The WorldHeart HeartSaver VAD uses both a tilting disc and a tissue valve. The Abiomed Biventricular Support (BVS) 5000 uses trileaflet valves made of polyurethane.[1]

Our group is currently developing a pneumatic ventricular assist device (PVAD). The flow that passes through the major orifice of the tilting disc valve acts on the blood pump at the diaphragm-housing junction,[2] creating a washout effect inside the blood pump that helps to prevent thrombosis. For this reason, we had previously developed a pulsatile PVAD with a tilting-disc valve. The majority of mechanical heart valves (MHVs) currently in clinical use are bileaflet valves with low-pressure gradients, central flow, and large effective orifice areas, and these devices have been demonstrated to exhibit hydrodynamic characteristics superior to those of tilting-disc valves.[3] At present, tilting-disc valves are no longer in common clinical use, and thus will be increasingly difficult to obtain in the future.

Thrombus formation and hemolysis within the blood pump were obstacles to the development of the VAD. Cavitation generated by valve closure is known to be a major cause of hemolysis.[4] Moreover, high shear stress in the downstream flow and the leaflet jet leakage are other major causes of hemolysis.[5] Cavitation has also been widely studied as being among the causes of MHV damage.[6–10] When the valve closes and local pressure falls below the vapor pressure of the liquid, cavitation bubbles form. When these bubbles collapse, higher pressure is generated by resultant shock waves and micro-jets. When the valve opens, high-speed flow and higher shear stress are generated, leading to blood cell trauma. A number of research groups have visualized the flow of MHVs under various physiological conditions.[11–15] The particle image velocimetry (PIV) method enables adequate temporal and spatial resolution to estimate flow velocity fields,[16] and thus is a powerful tool for studying this type of medical device. Kaminsky *et al.*[16] investigated the maximum flow velocity of a monoleaflet valve and a bileaflet valve using the PIV method, and they reported that the maximum flow velocity of a bileaflet valve reached 1.3 m/s. Reynolds shear stress (RSS) is often the main focus of investigations of MHV hemodynamics and the hemolysis caused by valve-induced flow turbulence.[5] Zhang *et al.*[17] investigated the RSS of a bileaflet valve under physiological conditions using the PIV method, and they reported that the maximum RSS reached 500 N/m^2 at peak systole.

In a previous study, we investigated the cavitation intensity for three different types of bileaflet valves.[14] However, the effects of shear stress due to bileaflet valves on the induction of hemolysis have not yet been investigated in detail. Therefore,

From the Department of Artificial Organs, Research Institute, National Cardiovascular Center, Fujishiro-dai, Suita, Osaka, Japan.

Presented in part 54th ASAIO Annual Conference, June 19–20, 2008 San Francisco, CA.

Submitted for consideration October, 2008; accepted for publication in revised form January, 2009.

Reprint Requests: Hwansung Lee, Department of Artificial Organs, Research Institute, National Cardiovascular Center 5-7-1, Fujishiro-dai, Suita, Osaka 565-8565, Japan. Email: hslee@ri.ncvc.go.jp.

DOI: 10.1097/MAT.0b013e3181a793e0

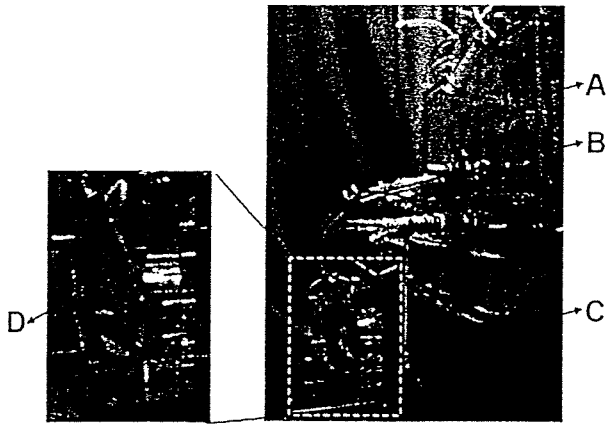

Figure 1. Configuration of the model pump. The model pump was made of acrylic resin to allow visualization of the flow velocity from the blood pump, the model pump had the same configuration as the PVAD. A: Donovan mock circulatory loop tester; B: ultrasound flow meter; C: model pump; D: valve mount.

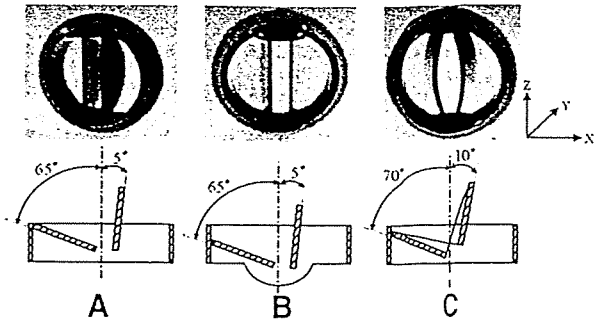

Figure 2. The bileaflet valves used in this study. A: ATS valve; B: St. Jude valve; C: Sorin Bicarbon valve.

in the present study, we investigated the shear stress of a bileaflet MHV causative of blood cell trauma. It is of note that the flow and shear-stress patterns may differ according to the hinge mechanism and the shape of leaflet used. To select the optimal bileaflet valve for the present PVAD, we used 2D PIV to investigate levels of Reynolds and viscous shear stress (VSS) downstream of three types of commercially available bileaflet valves.

Materials and Methods

Model Pump and Experimental Condition

The PVAD with a diaphragm was developed by the National Cardiovascular Center in Japan.[18] It has an outer diameter of 88 mm, a thickness of 47 mm, and a stroke volume of 75 ml. To visualize the flow inside the blood pump and downstream of the MHV in our PVAD,[19] a model pump unit was constructed of acrylic resin (**Figure 1**). The model pump was connected to a Donovan mock circulatory loop tester.[20] The mean aortic pressure and mean atrial pressures were maintained at 100 and 7 mm Hg, respectively, and were measured by a pressure transducer (MP5100; Baxter, Deerfield, IL) with a sampling frequency of 1 kHz. The model pump was operated at a positive pressure of 250 mm Hg and a negative pressure of −60 mm Hg with a control-drive console for circulatory support (VCT-30; Toyobo, Osaka, Japan). The model pump ran at a heart rate of 70 beats/min and a systolic duration of 35%, and the bypass flow was 4.2 L/min. The working fluid was a mixture of 50% distilled water and 50% glycerol by volume, and had a viscosity coefficient of 3.4 cP and a density of 1,120 kg/m^3 at 37°. Bypass flow was measured using an ultrasound flow meter (T106; Transonic Systems, Inc., Ithaca, NY) placed at the outflow side of the model pump (**Figure 1**).

Testing Valve

A 21-mm ATS valve (ATS Medical Inc., Minneapolis, MN), a 21-mm St. Jude 21-mm Sorin Bicarbon valve (Sorin Biomedica, Vercelli, Italy) were each mounted on the model pump after removing the sewing ring (Fi valve (St. Jude Medical, Inc., St. Paul, MN), and ag. 2). The ATS valve is a bileaflet valve with pyrolytic carbon housing and a pyrolytic carbon flat leaflet.[3] The ATS valve has a convex hinge mechanism which is designed to facilitate retrograde washing (**Figure 2A**). The St. Jude valve has flat leaflets which are orifice-oriented, and the closing forces are supported by the pivot system.[3] This pivot is raised above the housing and leaflet motion carried out by rotation (**Figure 2B**). The Sorin Bicarbon valve has titanium housing and curved leaflets made of pyrolytic carbon coated over a graphite and tungsten substrate.[3] The curved leaflets separate the orifice into three sections with similar resistance to flow, a similar low-pressure gradient, and minimal turbulence. Titanium housing strengthens the prosthesis, and the minimized thickness increases the effectiveness of the orifice (**Figure 2C**). The configuration of the bileaflet valves is shown in **Table 1**. Although the sewing ring diameter was identical in the three different bileaflet valves, they had different orifice and outer ring diameters once the sewing ring had been removed. To remove the effect of the inlet valve on the flow pattern inside of the model pump, a 21-mm Medtronic Hall valve (Medtronic, Inc., Minneapolis, MN) was used in the mitral position for each study. A charge-coupled device laser displacement sensor (LK-080, Keyence, Osaka, Japan) with a sampling frequency of 1 kHz was used to measure the opening and closing behavior of the leaflet (**Figure 3**).

PIV Method

A dual Nd:YAG laser system (Solo II-15, New Wave Research, Inc, Fremont, CA) with a 30 mJ/pulse at a 532-nm wavelength, and a pulse width of 3–5 ns was used for the flow visualization (**Figure 3**). The PIV images were taken by high-speed camera with 1,008 × 1,024 pixels and 9 μm/pixel square spacing (PIVCAM 10–30, TSI, Inc., Shoreview, MN). The camera was operated at a frame rate of 30 Hz, with a shutter-open time of 200 μs. A laser pulse delay (the amount of time that passes from the start of a pulse sequence to the first laser pulse) of 180 ms and a delta time (the time elapse between the first and second laser pulse) of 50 μs was fixed during the experiment.

The laser sheet illuminated two different planes, the X-Y plane and the X-Z plane. The flow velocity vector was measured using PIV software (Insight 3G; version 9.0, TSI, Inc., Shoreview, MN), and its vector files were loaded into the Tecplot Focus 2008 (Tecplot, Inc., Bellevue, WA) to present the PIV data graphically. We used a recursive Nyquist grid

Table 1. Configuration of Bileaflet Valves

Valves	Sewing Ring Diameter (mm)	Outer Ring Diameter (mm)	Orifice Diameter (mm)	Opening Angle (Degree)
A TS valve	21	18.2	14.8	60
St. Jude valve	21	18.4	14.7	60
Sorin Bicarbon valve	21	18.7	15.2	60

with a starting spot dimension of 64 × 64 pixels and a final spot dimension of 32 × 32 pixels. In addition, we used the Fast Fourier Transform correlate as the correlation engine, and the Gaussian peak as the peak engine. A polystyrene tracer with a diameter of 50 μm and a density of 1.06 g/cm^2 (Vestosint; Degussa AG, Düsseldorf, Germany) was added to the fluid.

To measure the flow velocity and RSS, a PIV image of 50 cycles was averaged for each of the experiment points. We employed a function generator to provide a square pulse, which was used as the trigger signal of the synchronizer (Model 610034, TSI, Inc., Shoreview, MN), and the electrocardiogram-R wave mode of the control-drive console was used for circulatory support (Figure 3). With a maximum flow velocity in the model pump of approximately 3 m/s and a camera resolution of 70 μm/pixel, a maximum displacement of 2.2 pixels was achieved.

The total shear stress is defined as

$$\tau = \tau^l + \tau^t \tag{1}$$

$$\tau^l = \mu\left(\frac{du}{dx} + \frac{dv}{dy}\right) \tag{2}$$

$$\tau^t = \rho\overline{u'v'} \tag{3}$$

where τ^l is the VSS and τ^t is the RSS. Moreover, μ is the viscosity coefficient and ρ is the density of the testing fluid. To investigate the possibility of blood cell damage, the Reynolds and VSS downstream of the three selected types of commercial bileaflet valves was measured by means of the 2D PIV method.

Results

The driving pressure, aortic pressure, valve behavior, and bypass flow waves are shown in Figures 4 and 5. The bypass flow was measured at the outflow side of the model pump (Figure 1). The square pulse of a function generator was used as the trigger signal of the control-drive console for circulatory support and the PIV synchronizer (Figure 4). Point "A" indicates the point at which the outlet valve opened, and "B" indicates the point at which the outlet valve closed. Outlet valve is opening between 325 and 375 ms, and is closing between 625 and 650 ms (Figure 5). There is no significant difference in valve behavior between the three kinds of bileaflet valves.

Images visualizing a valve are shown in Figure 6. Visualization of flow was carried out downstream of the MHV during the systolic phase. In the three types of bileaflet valves, high-flow velocity was observed at the upper and lower sides of the X-Y plane during the mid-systole and end-systole phase (between 425 ms and 575 ms in Figure 7, A–C). However, high-flow velocity was also observed along the central line of the X-Z plane during the mid-systole phase (between 475 ms and 525 ms in Figure 7, D–F). The maximum flow velocity occurred in the same location. The maximum flow velocities of the three kinds of bileaflet valves were plotted (Figure 8). The maximum flow velocity of the ATS and the St. Jude valves

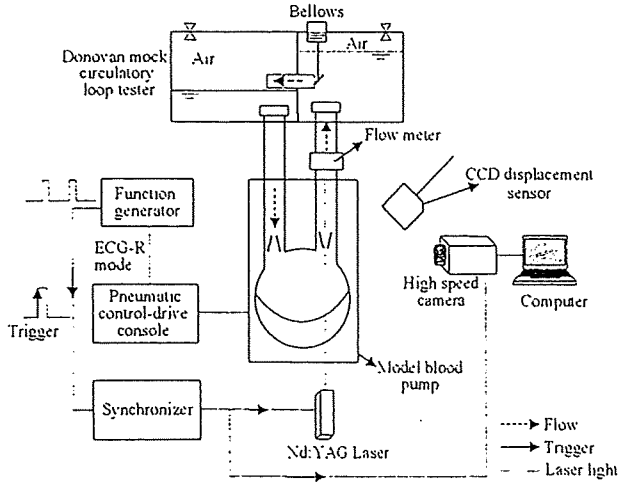

Figure 3. Diagram of the experimental system. We employed a function generator to provide a square pulse, which was used as the trigger signal of the synchronizer and the control-drive console.

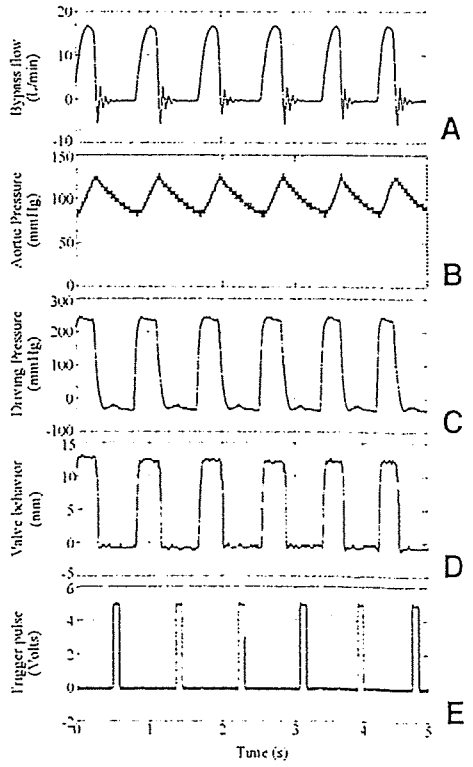

Figure 4. Driving pressure, aortic pressure, bypass flow, and trigger pulse waves in the Sorin Bicarbon valve on the X-Y plane. A: Bypass flow; B: Aortic pressure; C: Driving pressure; D: Outlet valve behavior; E: Trigger pulse of function generator.

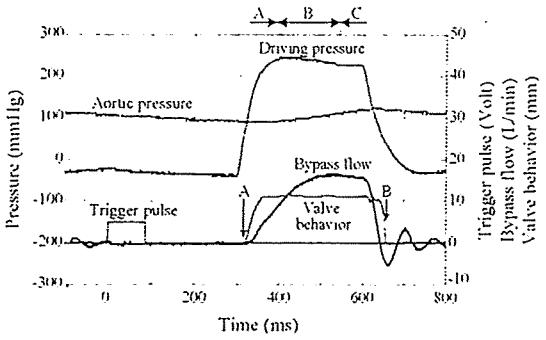

Figure 5. Example of the trigger timing of the PIV system. A: Early-systolic phase; B: Mid-systolic phase; C: End-systolic phase. In the Sorin Bicarbon valve, the waves on the X-Y plane are shown, and a time axial of 0 is the trigger point. A square pulse generated by a function generator was used to trigger the signals. Point "A" indicates the point at which the outlet valve opened, and "B" indicates the point at which the outlet valve closed.

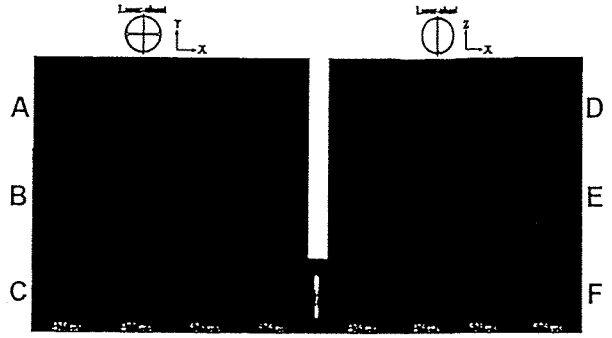

Figure 7. Vector field of the flow velocity. A: ATS valve on the X-Y plane; B: St. Jude valve on the X-Y plane; C: Sorin Bicarbon valve on the X-Y plane; D: ATS valve on the X-Z plane; E: St. Jude valve on the X-Z plane; F: Sorin Bicarbon valve on the X-Z plane.

remained above 2.0 m/s on the X-Y plane (Figure 8A). However, the maximum flow velocity of the Sorin Bicarbon valve only reached 2.0 m/s. However, no significant differences between the three kinds of bileaflet valves in terms of the maximum flow velocity along the X-Z plane were observed (Figure 8B).

With both the ATS and St. Jude valves, high RSS was observed at the wall and near the leaflet of the X-Y plane during all systole phases (Figure 9, A and B). In the case of the Sorin Bicarbon valve, high RSS was observed on the X-Y plane along the central line during the mid-systolic and end-systolic phase (between 475 ms and 575 ms in Figure 9C). In the case of both the ATS and St. Jude valves, high RSS was observed at the central line of the X-Z plane during all systolic phases (Figure 9, D and E). In the case of the Sorin Bicarbon valve, high RSS was also observed near the leaflet of the X-Z plane during the mid-systolic and end-systolic phases (between 425 ms and 575 ms in Figure 9F). High VSS was observed at the wall and near the leaflet of both the ATS and the St. Jude valves (Figure 10, A and B), and was observed at the central line of the Sorin Bicarbon valve in the X-Z plane. In the X-Z plane, high VSS was observed near the leaflet of all of the bileaflet valves tested (Figure 10, D–F). At the X-Z plane, the locations at which the maximum RSS and VSS occurred differed among the three types of bileaflet valves tested. However, in the X-Z plane, the maximum RSS and VSS values were observed at the same location in each valve tested.

The maximum RSS values of the three types of bileaflet valve were plotted (Figure 11). Along the X-Y plane, the RSS of the ATS valve and St. Jude valve reached above 200 N/m^2 during the mid-systole phase. However, the RSS of the Sorin Bicarbon valve reached 130 N/m^2. On the X-Z plane, the RSS of the ATS valve and St. Jude valve reached 250 N/m^2 during the mid-systole phase, a value which was higher than that achieved by the Sorin Bicarbon valve. For all three types of bileaflet valve, the RSS on the X-Z plane was higher than that on the X-Y plane (Figure 11). The maximum VSS values achieved by the three types of bileaflet valve were plotted (Figure 12). In all of the bileaflet valves, the maximum VSS value fell below 3 N/m^2, which was 1% of the maximum RSS.

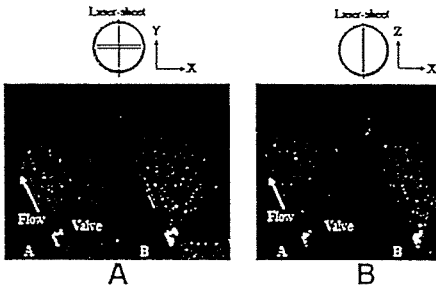

Figure 6. Images of the PIV system. A: X-Y plane; B: X-Z plane. The images shown are of the Sorin Bicarbon valve, and the duration is 500 ms. Image A was taken upon the first laser pulse, and image B was taken upon the second laser pulse. The time interval between images A and B was 50 μs.

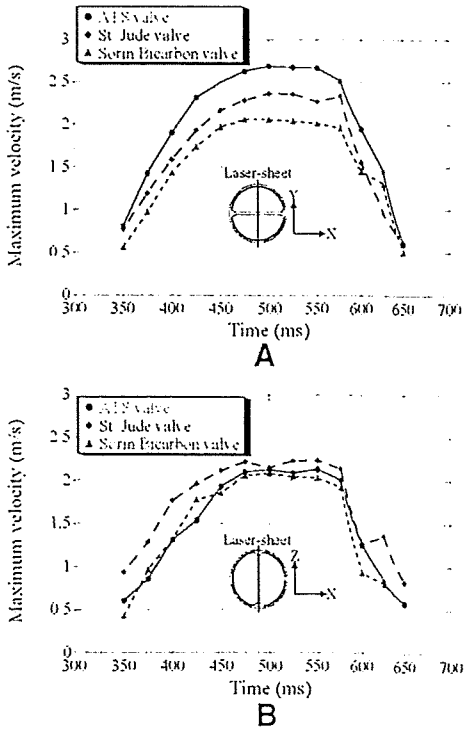

Figure 8. The maximum flow velocity during the systolic phase. A: X-Y plane; B: X-Z plane.

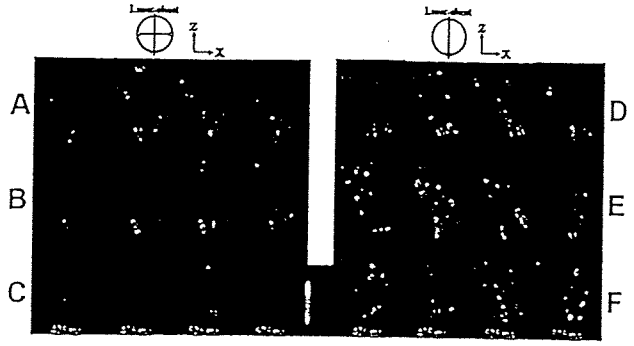

Figure 9. Pattern of the Reynolds shear stress. A: ATS valve on the X-Y plane; B: St. Jude valve on the X-Y plane; C: Sorin Bicarbon valve on the X-Y plane; D: ATS valve on the X-Z plane; E: St. Jude valve on the X-Z plane; F: Sorin Bicarbon valve on the X-Z plane.

Discussion

Among the causes of blood cell trauma is the cavitation phenomenon, which occurs at the mitral position in artificial hearts.[21,22] In our investigations of this phenomenon, we found that greater stress can be generated at the aortic position during the systolic phase. Therefore, investigation of the level of RSS in a PVAD remains quite important. In the present study, we used the PIV method to visualize the flow downstream of the outlet valve in a PVAD. Other groups have visualized the effects of flow on the sinus cavity[7–9,23] as well as examined the condition of an implantable MHV in a natural heart.[11,24] In the present study, we visualized the flow of an MHV in an artificial heart in which there was no sinus cavity, and the boundary conditions differed from those of a natural heart. Moreover, the flow velocity shapes differed from the shape of the leaflet (Figure 7). The Sorin Bicarbon valve is equipped with a thin layer of carbon on a titanium housing that enables the orifice to be effective. Although the three types of valve tested here have identical sewing ring diameters, the orifice diameter differs: the diameter of the orifice on the Sorin Bicarbon valve is larger than that of the other two valves, i.e., the orifice diameter of the Sorin Bicarbon valve is 15.2 mm, that of the ATS valve is 14.8 mm, and that of the St. Jude valve is 14.7 mm (Table 1). The larger orifice diameter of the Sorin Bicarbon valve accounted for the maximum flow velocity (Figure 7C).

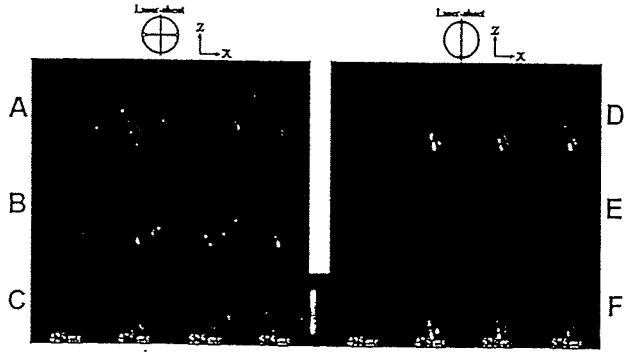

Figure 10. Pattern of viscous shear stress. A: ATS valve on the X-Y plane; B: St. Jude valve on the X-Y plane; C: Sorin Bicarbon valve on the X-Y plane; D: ATS valve on the X-Z plane; E: St. Jude valve on the X-Z plane; F: Sorin Bicarbon valve on the X-Z plane.

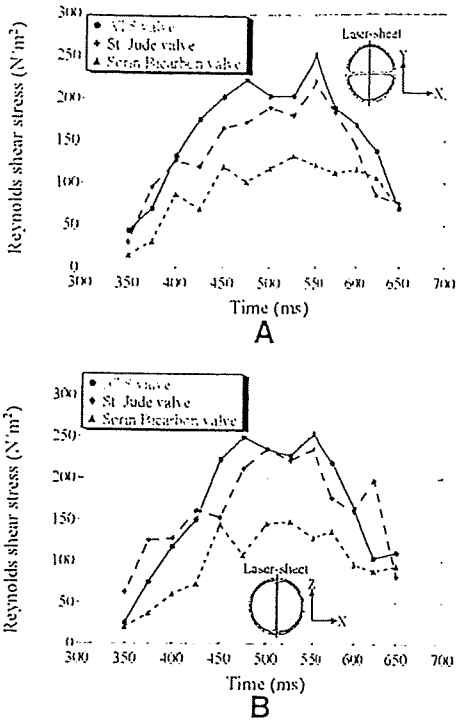

Figure 11. Maximum Reynolds shear stress during the systolic phase. A: X-Y plane; B: X-Z plane.

Even though the ATS and St. Jude valves possess flat leaflets, the pivot of the St. Jude valve is raised above the housing (Figure 3), which yields a different maximum flow velocity on the X-Y plane (Figure 8A). However, because these two bileaf-

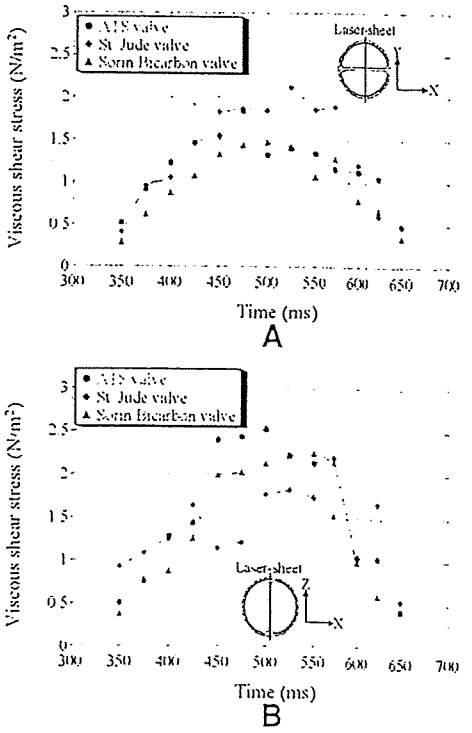

Figure 12. Maximum viscous shear stress during the systolic phase. A: X-Y plane; B: X-Z plane.

let valves possess flat leaflets, they do not exhibit a significant difference in the maximum RSS (Figure 11). On the X-Y plane, the greater RSS of the flat leaflet was observed at the wall (Figure 9, A and B), but the higher RSS of the curved leaflet was observed along the central line (Figure 9C). In the case of the MHV, a wake was created by the streamlined leaflet.[10] The wake of the flat leaflet was strong, which yielded a high-flow velocity (Figure 7, A and B) as well as high RSS at the wall (Figure 9, A and B).

Hemolysis (red cell damage and platelet damage) is a function of exposure time and shear stress.[25] Leverett *et al.*[6] have reported that the threshold level for blood cell damage due to shear stress is approximately 150 N/m^2, and an exposure time of 102 s. Sallam and Hwang[26] reported that hemolysis requires shear stress of 400 N/m^2 during exposure time of 1 ms through a heart valve, and sublethal damage to red cells can occur at a turbulence shear stress of 50 N/m^2. In the present study, values were fixed at a heart rate of 70 beats/min and a systolic duration of 35%, such that the systolic time was 300 ms, and the maximum RSS of the bileaflet valves reached 250 N/m^2. However, as shown in Figure 12, the maximum VSS value was found to be well below that associated with blood cell damage, and was also below the experimental determined threshold of approximately 10 N/m^2 required for platelet damage.[5,6] The maximum RSS values of the three types of bileaflet valve were smaller than those of the hemolysis threshold previously reported by other groups.[6,26] The present RSS values exceeded the threshold of sublethal damage to red cells, i.e., 50 N/m^2. As shown in Equation 1, hemolysis in the bileaflet valves in our PVAD would be possible, if the total shear stress were considered. However, the maximum RSS during the systolic phase in the Sorin Bicarbon valve was less than that of either the ATS or the St. Jude valve. Moreover, in a previous study, we reported less cavitation intensity with the Sorin Bicarbon valve than with either the ATS or the St. Jude valve.[14] In general, cavitation and high-shear stress at a MHV are major causes of hemolysis.[4,5] If the possibility of hemolysis is given high priority, the Sorin Bicarbon valve would be considered the best valve among the three valves tested for our PVAD.

To decrease the error, the model pump was run under full filling and full ejection conditions. Moreover, the heart rate was fixed at the low rate of 70 bpm. However, in this study, the standard error in the maximum flow velocity was found to be 5.5%, and the standard error in the RSS and VSS was approximately 20%, as based on a 5.5% random error of the flow velocity. To also investigate optical distortion, we measured the flow velocity under nonflow conditions. We observed a mean flow velocity of 0.02 m/s under the nonflow conditions, which has below 1% of the maximum flow velocity of 2.8 m/s. It is possible that differences in the density of the working fluid and the polystyrene tracer exerted some effects on the present results.

The present study was restricted to observation of flow downstream of bileaflet valves, and thus did not address other points of interest such as the hinge gaps and the leaflet leakage jet. In general, very high-shear stress was generated at the gap between the valve housing, the leaflet, and the valve hinge during the leaflet closure phase. Because the valve housing and the leaflet are made of pyrolytic carbon and titanium, it was difficult to carry out flow visualizing at hinge, and gap between the housing and leaflet (Figure 2). Therefore, in future studies, we will analyze the hemodynamics of hinge gaps and leakage jets using a model valve composed of acrylic resin. The development of a VAD must also include a consideration of thrombus formation inside of the blood pump. In the present study, we did not visualize the flow in the blood pump using a bileaflet valve. In future studies, a bileaflet valve should be employed with a pulsatile VAD. To make the best selection, we initially investigated the RSS and cavitation intensity[18] of a bileaflet valve in our PVAD. As a next step, we will visualize the flow inside of the blood pump.

Conclusion

In the present study, we visualized flow through bileaflet valves using the PIV method. Here, we observed high flow velocity near the leaflet during the systolic phase. The Sorin Bicarbon curved-leaflet valve created a substantial central flow that reduced turbulence and in turn reduced overall flow velocity.

The maximum VSS was found to be only 1% of the maximum RSS. Thus, the effect of VSS on blood cell trauma could be neglected. Although the bileaflet valves tested here were very similar in design, the flow velocity and RSS patterns differed according to the shape of the leaflet. Of the three valves tested here, the Sorin Bicarbon valve was found to yield the lowest level of RSS, and was thus considered to be the best valve for our PVAD.

Acknowledgment

Supported by the Program for the Promotion of Fundamental Studies in the Health Sciences of the National Institute of Biomedical Innovation (NIBIO).

References

1. Stevenson LW, Kormos RL: Mechanical cardiac support 2000: Current applications and future trial design. *J Heart Lung Transplant* 20: 1–38, 2001.
2. Nakata M, Masuzawa T, Tatsumi E, *et al*: Characterization and optimization of the flow pattern inside a diaphragm blood pump based on flow visualization techniques. *ASAIO J* 44: M714–M718, 1998.
3. Jamieson WR: Advanced technologies for cardiac valvular replacement, transcatheter innovations and reconstructive surgery. *Surg Technol Int* 15: 149–187, 2006.
4. Kafesjian R, Howanec M, Ward GD, *et al*: Cavitation damage of pyrolytic carbon in mechanical heart valves. *J Heart Valve Dis* 3: S2–S7, 1994.
5. Ge L, Dasi LP, Sotiropoulos F, Yoganathan AP: Characterization of hemodynamic forces induced by mechanical heart valve: Reynolds vs. viscous stresses. *Ann Biomed Eng* 36: 276–297, 2007.
6. Leverett LB, Hellums JD, Alfrey CP, Lynch EC: Red blood cell damage by shear stress. *Biophys J* 12: 257–273, 1972.
7. Liu JS, Lu PC, Lo CW, *et al*: An experimental study of steady flow patterns of a new trileaflet mechanical aortic valve. *ASAIO J* 51: 336–341, 2005.
8. Lim WL, Chew YT, Chew TC, Low HT: Pulsatile flow studies of a porcine bioprosthetic aortic valve in vitro: PIV measurements and shear-induced blood damage. *J Biomech* 34: 1417–1427, 2001.
9. Grigioni M, Daniele C, D'Avenio G, Barbaro V: The influence of the leaflets' curvature on the flow field in two bileaflet prosthetic heart valves. *J Biomech* 34: 613–621, 2001.
10. Goubergrits L, Affeld K: Numerical estimation of blood damage in artificial organs. *Artif Organs* 28: 499–507, 2004.
11. Akutsu T, Saito J: Dynamic particle image velocimetry flow anal-

ysis of the flow field immediately downstream of bileaflet mechanical mitral prostheses. *J Artif Organs* 9: 165–178, 2006.
12. Castellini P, Pinotti M, Scalise L: Particle image velocimetry for flow analysis in longitudinal planes across a mechanical artificial heart valve. *Artif Organs* 28: 507–513, 2004.
13. Subramanian A, Mu H, Kadambi JR, *et al*: Particle image velocimetry investigation of intravalvular flow fields of a bileaflet mechanical heart valve in a pulsatile flow. *J Heart Valve Dis* 9: 721–731, 2000.
14. Lee HS, Homma A, Taenaka Y: Hydrodynamic characteristics of bileaflet mechanical heart valve in an artificial heart: cavitation and closing velocity. *Artif Organs* 31: 532–537, 2007.
15. Heise M, Schmidt S, Krüger U, *et al*: Flow pattern and shear stress distribution of distal end-to-side anastomoses. A comparison of the instantaneous velocity fields obtained by particle image velocimetry. *J Biomech* 37: 1043–1051, 2004.
16. Kaminsky R, Kallweit S, Weber HJ, et al: Flow visualization through two types of aortic prosthetic heart valves using steroscoptic high-speed particle image velocimetry. *Artif Organs* 31: 869–879, 2007.
17. Zhang P, Yeo JH, Qian P, Hwang NHC: Shear stress investigation across mechanical heart valve. *ASAIO J* 53: 530–536, 2007.
18. Lee HS, Taenaka Y: Characteristics of mechanical heart valve cavitation in a pneumatic ventricular assist device. *Artif Organs* 32: 453–460, 2008.
19. Akagawa E, Lee HS, Tatsumi E, *et al*: Effects of mechanical valve orifice direction on flow pattern in a ventricular assist device. *J Artif Organs* 10: 85–91, 2007.
20. Donovan FM Jr: Design of a hydraulic analog of the circulatory system for evaluating artificial hearts. *Biomater Med Devices Artif Organs* 3: 439–449, 1975.
21. Lee HS, Tsukiya T, Homma A, *et al*: Observation of cavitation bubbles in monoleaflet mechanical heart valves. *J Artif Organs* 7: 121–127, 2004.
22. Lee HS, Taenaka Y, Kitamura S: Mechanisms of mechanical heart valve cavitation in an electrohydraulic total artificial heart. *ASAIO J* 51: 208–213, 2005.
23. Medart D, Schmitz C, Rau G, Reul H: Design and in vitro performance of a novel bileaflet mechanical heart valve prosthesis. *Int J Artif Organs* 28: 256–263, 2005.
24. Lu PC, Liu JS, Huang RH, *et al*: The closing behavior of mechanical heart valve prostheses. *ASAIO J* 50: 294–300, 2004.
25. Graf T, Reul H, Dietz W, *et al*: Cavitation of mechanical heart valves under physiologic conditions. *J Heart Valve Dis* 1: 131–141, 1992.
26. Sallam AM, Hwang NHC: Human red blood cell hemolysis in a turbulence shear flow: contribution of Reynolds shear stresses. *Biorheology* 21: 783–797, 1984.

Effects of the Driving Condition of a Pneumatic Ventricular Assist Device on the Cavitation Intensity of the Inlet and Outlet Mechanical Heart Valves

HWANSUNG LEE, EISUKE TATSUMI, AND YOSHIYUKI TAENAKA

Our group is currently developing a pneumatic ventricular assist device (PVAD), and in previous studies, we reported the mechanical heart valve (MHV) cavitation intensity at the inlet valve in the PVAD only. In this study, we investigated the effect of the running conditions on the cavitation intensity both for the inlet and outlet valve in the PVAD using an acoustic signal. A 23-mm Medtronic Hall valve with an opening angle of 70° was mounted in the inlet and outlet port of the PVAD after removing the sewing ring. A mini pressure sensor with high frequency was mounted 15 mm downstream from the inlet valve and downstream from the outlet valve. The pressure signal was band-pass filtered between 35 and 500 kHz using a digital filter. The band-pass filtered root mean squared (RMS) pressure was used as an index of the cavitation intensity. The RMS pressure of the inlet valve was higher than that of the outlet valve. Even if the outlet valve has a lower RMS pressure than the inlet valve, cavitation occurs. In case of a full-filling and full-ejection condition, the RMS pressure of the inlet valve was higher than that of the partial-filling and partial-ejection condition. This means that a partial-filling and partial-ejection condition is best to prevent the hemolysis caused by the cavitation phenomenon and the damage to the valve surface in our PVAD system. *ASAIO Journal* 2009; 55:328–334.

Cavitation is the rapid formation and collapse of vapor-filled cavities that occurs when a fluid is exposed to rapid changes in pressure below liquid-vapor pressure.[1] When cavitation occurs near the material surface of a mechanical heart valve (MHV), this rapid collapse may cause the generation of a high-speed microjet and shock waves, resulting in the generation of high pressure. This high pressure might cause blood cell damage and valve failure. Cavitation is a major cause of pits on the valve surface, which decrease the durability of the MHV. Kornberg *et al.*[2] observed leaflet escape due to a strut fracture at 42 months after implantation of a monoleaflet MHV. Klepetko *et al.*[3] observed microscopic pitting on a bileaflet valve at 36 and 38 months after implantation. Those pyrolytic carbon fractures seemed to be primarily the result of the cavitation phenomenon.

Wide-ranging high-frequency pressure fluctuation due to collapse of the cavitation bubbles has occurred.[4] A valve resonance ranged below 35 kHz, and cavitation bubbles could only be observed when pressure signals were at frequencies above 35 kHz.[4] In a previous study, the root mean squared (RMS) pressure and cavitation cycle duration increased with the closing velocity of the inlet valve of a pneumatic ventricular assist device (PVAD).[5] Moreover, we attempted to perform a synchronized analysis between the visual images of the cavitation and acoustic signals in the inlet valve of the PVAD.[6] We reported that a high-frequency signal wave was generated when the bubbles collapsed.[6]

An inlet valve was closed by the slope of the ventricular pressure during systolic phase. Conversely, an outlet valve was closed by the slope of the aortic pressure during diastolic phase. In general, slope of the ventricular pressure during systolic phase was higher than that of the aortic pressure during diastolic phase. The cavitation of the inlet valve was more severe than that of the outlet valve; therefore, the cavitation intensity of the mitral position valve was investigated in many groups.[7–10] In our previous studies, we investigated the MHV cavitation of an inlet valve in the PVAD.[11,12] Lukic *et al.*[13] reported the cavitation intensity in the outlet valve of a pediatric pulsatile ventricular assist device. Even if the RMS pressure of the outlet valve was less than that of the inlet valve, there is a possibility of cavitation in the outlet valve.[13] In a previous study, we did not investigate the cavitation in an outlet valve in the PVAD; however, cavitation can occur.

To investigate the effect of the running conditions on the cavitation intensity of both the inlet and outlet valve in the PVAD, we used the RMS pressure after band-pass filtering using a digital filter as an index of the cavitation intensity. In the previous study, we selected the Medtronic Hall valve as the MHV, which has a good washout effect inside the blood pump, resulting in the prevention of thrombosis.[14] The RMS pressure was investigated at the various heart rate and systolic duration.

Materials and Methods

The PVAD with a diaphragm was developed by the National Cardiovascular Center in Japan (**Figure 1**). It has an outer diameter of 88 mm, a thickness of 47 mm, and a stroke volume

From the Department of Artificial Organs, Research Institute, National Cardiovascular Center, Osaka, Japan.

Submitted for consideration August 2008; accepted for publication in revised form February 2009.

Reprint Requests: Hwansung Lee, PhD, Department of Artificial Organs, Research Institute, National Cardiovascular Center, 5-7-1, Fujishirodai, Suita, Osaka 565-8565, Japan. Email: hslee@ri.ncvc.go.jp.

DOI: 10.1097/MAT.0b013e3181a8d84f

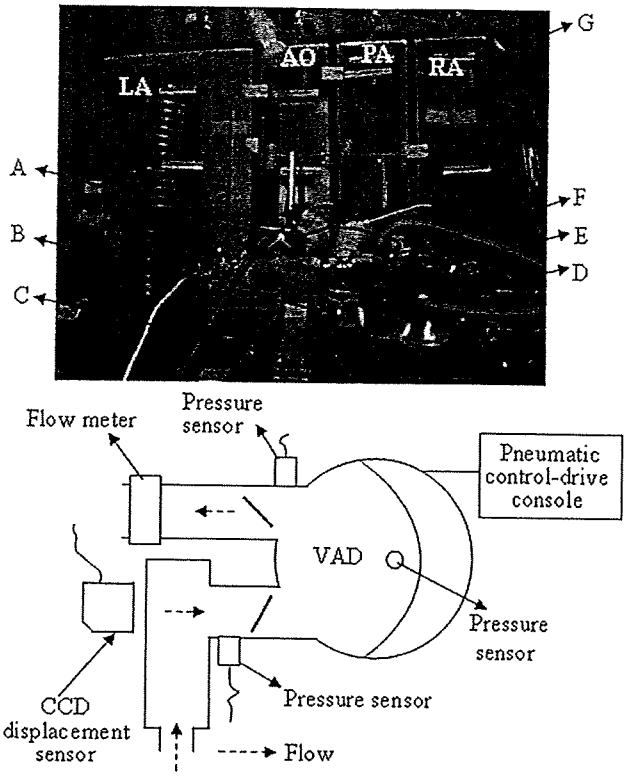

Figure 1. Photograph of the pneumatic ventricular assist device (PVAD) and diagram of the experiment system. Ultrasonic flow meter (**A**), pressure sensor of inlet valve (**B**), acrylic resin chamber (**C**), detect port of the ventricular pressure (**D**), PVAD (**E**), pressure sensor of outlet valve (**F**), and Donovan mock circulatory loop tester (**G**). LA, left atrium chamber, AO, aortic chamber, PA, pulmonary arterial chamber, RA, right atrium chamber. Our PVAD has an outer diameter of 88 mm, a thickness of 47 mm, and a stroke volume of 75 ml. A function generator was employed to provide a square pulse and used as the trigger signal for the control-drive console. In addition, this square pulse was delayed by a delay circuit and used as the trigger signal for the pressure sensor.

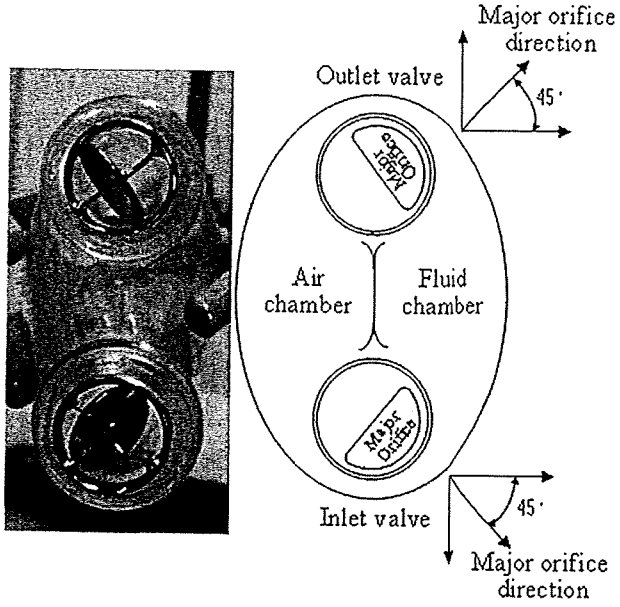

Figure 2. Valve orientation angle. For the inlet valve, the major orifice direction was set at a 45° clockwise orientation. In contrast, for the outlet valve, these angles were set at a 45° counterclockwise orientation.

of 75 ml.[14] A 23-mm Medtronic Hall valve (Medtronic, Inc., Minneapolis, MN) with an opening angle of 70° was mounted in the inlet and outlet valve position after removing the sewing ring. The PVAD was connected to a Donovan mock circulatory loop tester.[15] It consisted of four chambers, such as right atrium, pulmonary, arterial, and left atrium (**Figure 1**). The Fluid flows from the right atrium chamber (RA) to the right blood pump, is pumped into the pulmonary arterial chamber (PA), flows through the pulmonary resistance valve into the left atrium chamber (LA), flows into the left blood pump, is pumped into the aortic chamber (AO), and is returned to the RA by flowing against system resistance (**Figure 1**).

Our PVAD was operated at a positive pressure ranging from 190 to 240 mm Hg and a negative pressure ranging from −40 to −70 mm Hg with a control-drive console for circulatory support (VCT-30; Toyobo, Osaka, Japan). The PVAD was run at heart rates ranging from 60 to 90 beats/min and systolic duration ranging from 37% to 43%. The mean aortic and atrial pressures were maintained at 100 mm Hg and 7 mm Hg, respectively. The blood analog fluid was a mixture of 50% water and 50% glycerol by volume, which has a viscosity coefficient of 3.4 cP, a density of 1.12 g/cm^3, and a vapor pressure of −715 mm Hg at 37°C. The fluid viscosity and vapor pressure were identical to those of blood at body temperature.[16]

To detect the inlet valve behavior, a charge-coupled device (CCD) laser displacement sensor (LC-2450; Keyence, Osaka, Japan) with a frequency sampling rate of 50 kHz was placed on top of the chamber made of acrylic resin. A miniature pressure sensor (M132A31; PCB Piezotronics, Depew, NY) with a resonance frequency of 1 MHz was mounted 15 mm away from the inlet and outlet valve surface. The data were stored using a digital oscilloscope (DL1640L; Yokogawa, Tokyo, Japan) at a 5 MHz sampling rate. The driving pressure and ventricular pressure of our PVAD were measured by a pressure transducer (MP5100; Baxter, Deerfield, IL) with a sampling frequency of 1 kHz. The pressure signal was band-pass filtered between 35 and 500 kHz using a digital filter (Labview 7.0; National Instruments, Austin, TX). Bypass flow was measured with an ultrasound flow meter (T106; Transonic System, Ithaca, NY) at the outflow side of the model pump (**Figure 1**). For the inlet valve, the major orifice direction of the Medtronic Hall valve was set at a 45° clockwise orientation. In contrast, for the outlet valve, these angles were set at a 45° counterclockwise orientation (**Figure 2**).

Statistical analyses were performed with a commercially available software package (Statview 5.0; SAS Institute, Cary, NC). The data were compared using the unpaired t test and factorial analysis of variance. Significance was based on a p value of 0.05 or less. All experiments are repeated at 50 times, and all data values are expressed as means ± SD.

Results

The bypass flow of the PVAD ranges from 4.0 to 6.0 L/min (**Figure 3**). The pump performs the ful-filling and the full-ejection condition at 40% of the systolic duration, resulting in the peak flow (**Figure 3**).

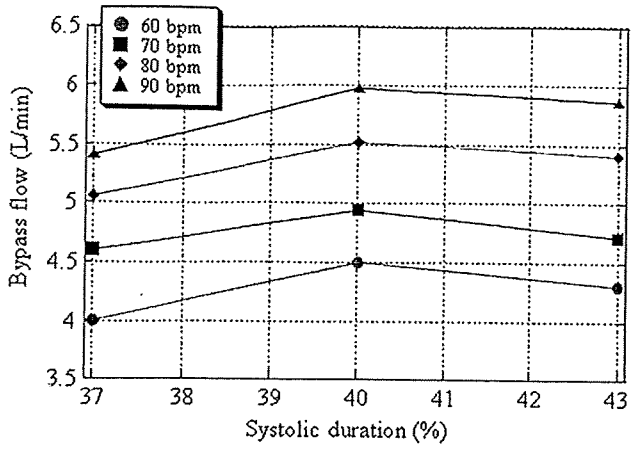

Figure 3. Bypass flow at various heart rates and systolic durations.

The pressures and bypass flow waves are shown in **Figure 4** and **5**. At a partial-filling and partial-ejection condition (heart rate of 70 beats/min and systolic duration of 37%), the ventricular pressure (equal to the pressure inside the pump) had three peak pressures (V_1, V_2, and V_3 in **Figure 4A**). The first and second peak occurred just before inlet valve closure (V_1 and V_2 in **Figure 4A**), and the third peak occurred after inlet valve closure (V_3 in **Figure 4B**). The point "B_1" of the valve behavior wave is the inlet valve closure, and "B_2" is the outlet valve closure (**Figure 4C**). The points "I_1" and "O_1" of the inlet and outlet valve pressure waves indicate the inlet valve closure, and "O_2" indicates the outlet valve closure (**Figure 4, D and E**). Conversely, at a full-filling and full-ejection condition (heart rate of 70 beats/min and systolic duration of 40%), the ventricular pressure has two peak pressures (V_1 and V_2 in **Figure 5A**), the first peak occurred just before the inlet valve closure (V_1 in **Figure 5B**). The point "B_1" of the valve behavior wave is the first inlet valve closure, and "B_2" is the secondary inlet valve closure point caused by the valve rebound. "B_3" is the outlet valve closure point (**Figure 5C**). "I_1" and "I_2" of the inlet valve pressure wave indicate the first and second inlet valve closure points, respectively. "I_3" indicates the reflective pressure resulting in the closing of the outlet valve (**Figure 5D**). "O_1" and "O_2" of the outlet valve pressure wave indicate the reflective pressure resulting in the first and second inlet valve closures, respectively (**Figure 5E**). "O_3" indicates the outlet valve closure point, which is the same point as "I_3".

The inlet valve-closing velocity during 5 ms, just before valve closure, is shown in **Figure 6**. The inlet valve-closing velocity increase with increases in the heart rate, and then reached a peak at the heart rate of 80 beats/min. At all heart rates, the inlet valve-closing velocity reached a peak at the systolic duration of 40%. At a low-systolic duration, the closing velocity ranged from 0.73 ± 0.1 to 0.97 ± 0.08 m/s. At a high-systolic duration, the closing velocity ranged from 0.96 ± 0.08 to 1.13 ± 0.13 m/s. In all heart rate, there were significant differences in the valve-closing velocity between a low- and high-systolic duration.

The unfiltered and filtered pressure signals are shown in **Figure 7**. At a full-filling and full-ejection condition, the frequency at the inlet valve is higher than that at the outlet valve (**Figure 7**). The filtered pressure signal between 35 and 500 kHz of high heart rate and high-systolic duration is higher than those at low heart rate and low-systolic duration.

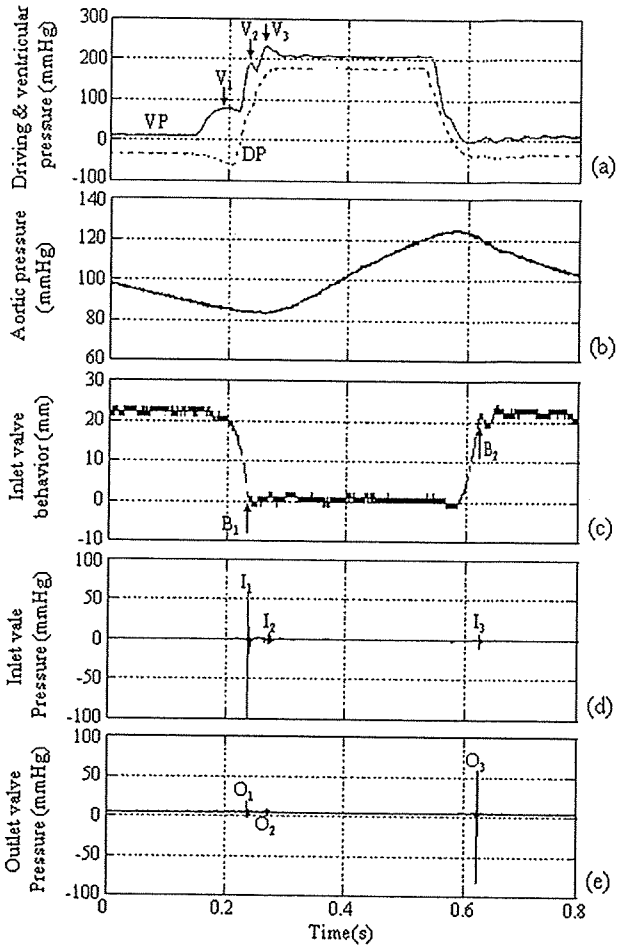

Figure 4. Pressure wave, bypass flow, and valve behavior motion with heart rate of 70 beats/min and systolic duration of 37%. Driving and ventricular pressure (**A**), aortic pressure (**B**), valve behavior motion (**C**), pressure near the inlet valve (**D**), pressure near the outlet valve (**E**). V_1, V_2, V_3: peak ventricular pressure during systolic duration; B_1: inlet valve closure; B_2: outlet valve closure; I_1: pressure near the inlet valve caused by inlet valve closure; I_2: pressure near the inlet valve caused by rebound; I_3: reflection pressure near the inlet valve caused by the outlet valve closure; O_1, O_2: reflection pressure near the outlet valve caused by the inlet valve closure and rebound; O_3: pressure near the outlet valve caused by the outlet valve closure.

The RMS pressure of the inlet valve increases as the heart rate and systolic duration increased (**Figure 8A**). The RMS pressure of the inlet valve reached a peak at the systolic duration of 40% in all heart rates. At a low-systolic duration, the RMS pressure of the inlet valve ranged from 12.53 ± 1.08 to 21.92 ± 3.14 mm Hg. At a high-systolic duration, the RMS pressure of the inlet valve ranged from 24.94 ± 3.57 to 27.45 ± 2.67 mm Hg. In all heart rate, there were significant differences in the RMS pressure of the inlet valve between a low- and high-systolic duration. Conversely, there was no change in the RMS pressure of the outlet valve (**Figure 8B**). At a low-systolic duration, the RMS pressure of the outlet valve ranged from 16.77 ± 0.82 to 19.69 ± 1.61 mm Hg. At a high-systolic duration, the RMS pressure of the outlet valve ranged from 15.47 ± 1.26 to 20.23 ± 1.44 mm Hg, which was less than that of the inlet valve. There were no significant

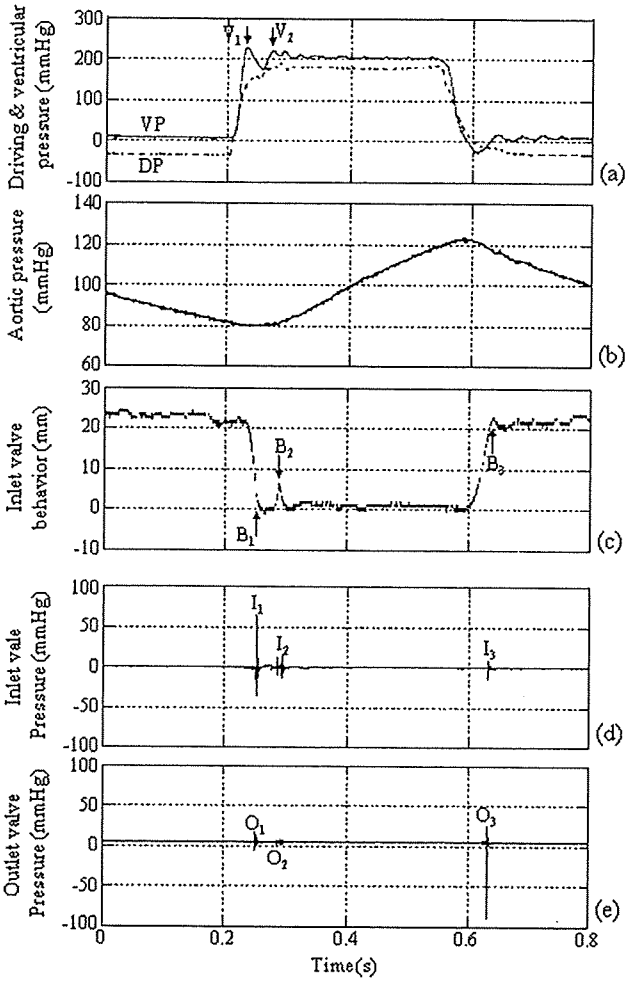

Figure 5. Pressure wave, bypass flow, and valve behavior motion with heart rate of 70 beats/min and systolic duration of 40%. Driving and ventricular pressure (**A**), aortic pressure (**B**), valve behavior motion (**C**), pressure near the inlet valve (**D**), pressure near the outlet valve (**E**). V_1, V_2: peak pressure of the ventricular during systolic duration; B_1: first inlet valve closure; B_2: secondary inlet valve closure; B_3: outlet valve closure; I_1: pressure near the inlet valve caused by inlet valve closure; I_2: pressure near the inlet valve caused by rebound; I_3: reflection pressure near the inlet valve caused by the outlet valve closure; O_1, O_2: reflection pressure near the outlet valve caused by the inlet valve closure and rebound; O_3: pressure near the outlet valve caused by the outlet valve closure.

differences in the RMS pressure of the inlet valve between a low- and high-systolic duration.

The pressure due to closing of the inlet valve and the outlet valve can be calculated from **Figure 9**,

$$P_{ic} = P_{ven} - P_{atr} \quad (1)$$

$$P_{oc} = P_{ao} - P_{ven} \quad (2)$$

where, P_{ic} and P_{oc} is the pressure causing the inlet valve and outlet valve closure, respectively. P_{ven} is the positive and/or negative peak ventricular pressure just before valve closure, P_{atr} is the atrial pressure, and P_{ao} is the aortic pressure.

The ventricular pressure just before inlet valve and outlet valve closure is shown in **Figure 10**. The ventricular pressure differs from the filling and ejecting condition of the blood

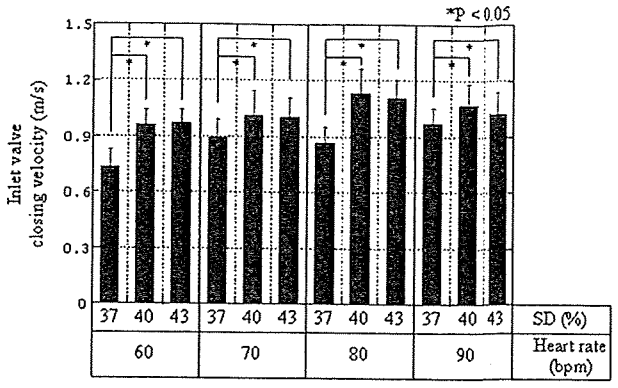

Figure 6. Closing velocity of the inlet valve. The inlet valve-closing velocity is the average velocity during the 5 ms just before valve closure.

pump. CP_i and CP_o indicate the inlet valve and outlet valve closure point, respectively. The static pressure difference (P_{ic} and P_{oc}) and inlet valve-closing velocity are shown in **Figure 11**. It has a tendency to linearly increase with increases in the RMS pressure.

Discussion

Many groups have estimated the MHV cavitation intensity using the band-pass filtered RMS pressure and the high-intensity transient signals (HIT).[17–22] Our group reported the MHV cavitation intensity in the PVAD using a synchronized analysis of the cavitation images and the acoustic signal of the cavitation bubbles.[12] We investigated the cavitation intensity of the inlet valve in our PVAD only. Therefore, in this study, we investigated the cavitation intensity of both the inlet valve and outlet valve using the RMS pressure.

Several groups have examined the maximum and average ventricular pressure slope (*dp/dt*), and they have used it as the loading index of the cavitation threshold.[23,24] However, as shown in **Figure 4** and **5**, the shape of the ventricular pressure differs from the running condition for the blood pump. The ventricular pressure slope cannot be used as the index of the MHV cavitation threshold for the PVAD, and we, therefore, used the driving pressure slope, just before valve closure, as the parameter for the MHV cavitation intensity[5] only under the full-filling and full-ejection conditions. However, this method was not valid for the partial-filling and partial-ejection condition. Therefore, in this study, we considered the pressure difference when estimating the cavitation intensity as another method. As shown in **Figure 10**, the pressure difference (P_{ic} and P_{oc}) has a tendency to linearly increase with increases in the RMS pressure. Moreover, in a previous study, we reported that the RMS pressure has a tendency to linearly increase with increases in the inlet valve-closing velocity.[12] It was concluded that it is valid to use the pressure difference to estimate the MHV cavitation intensity in our PVAD system, and that the success using the pressure difference shows that the cavitation intensity was not dependent on the filling and ejection condition, but rather on the valve-closing velocity.

Moreover, several articles have indicated that a full-filling and full-ejection condition decrease cavitation intensity.[17,26,27] However, as shown in **Figure 8A**, the partial-filling and partial-

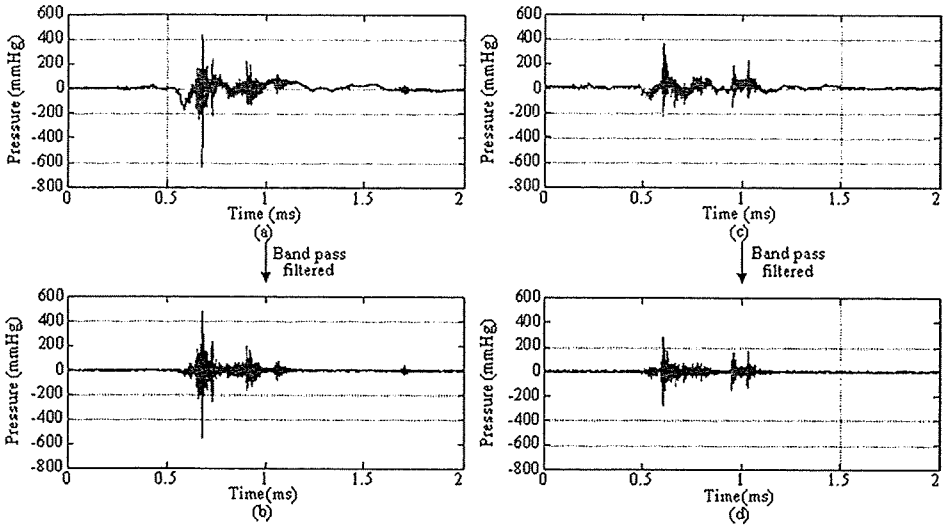

Figure 7. Pressure signal at a heart rate of 70 beats/min and systolic duration of 40%. Pressure signal at the inlet valve (A), band-pass filtered signal at the inlet valve (B), pressure signal at the outlet valve (C), and band-pass filtered signal at the outlet valve (D). The pressure signal was band-pass filtered between 35 and 500 kHz using a digital filter.

ejection condition of the blood pump decreased the RMS pressure, which is an index of the cavitation intensity. This contradicted the results by other groups. We think that this contradiction may be related to the difference in the mechanism of the blood pump and the pump size. Lukic *et al.*[13] used the pediatric pulsatile VAD with a 15 ml stroke volume, whereas Zapanta *et al.*[26] used the electrical VAD of the pusher-plate type. Our pneumatic VAD was a diaphragm type, in which the ventricular pressure suddenly increased during the systolic phase. Cavitation bubbles were found to be concentrated on the valve stop of the Medtronic Hall valve.[5,12] The observation areas and visual time of the cavitation bubbles increased as the valve-closing velocity increased. This means that the major cause of the cavitation was determined to be the squeeze flow that can take place in the narrow gap between the leaflet and valve stop. The cavitation intensity is closely related to the valve-closing velocity but in what way does the squeeze flow related to this fact. In this study, we confirmed that the slope of the ventricular pressure under the full-filling

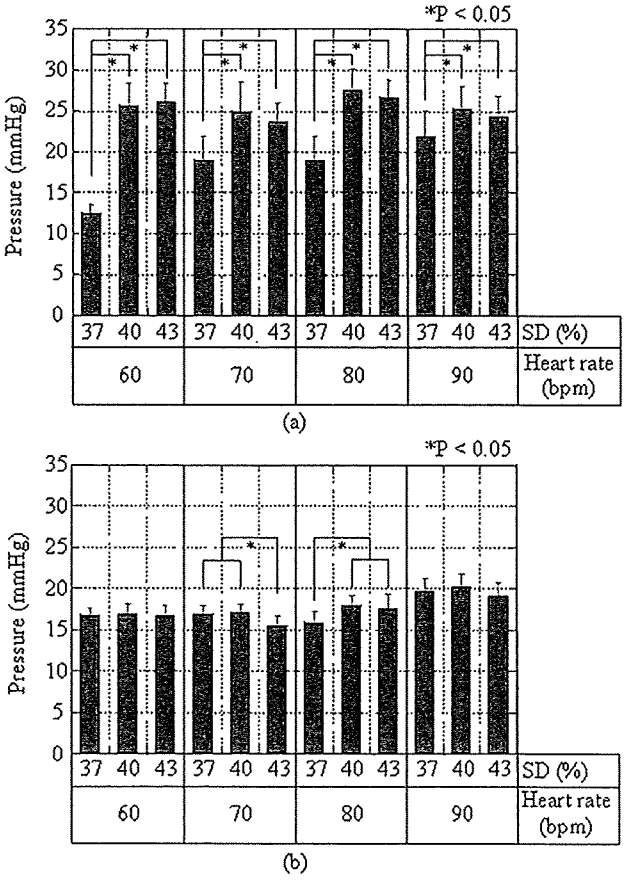

Figure 8. RMS pressure after band-pass filtered between 35 and 500 kHz. Inlet valve (A) and outlet valve (B).

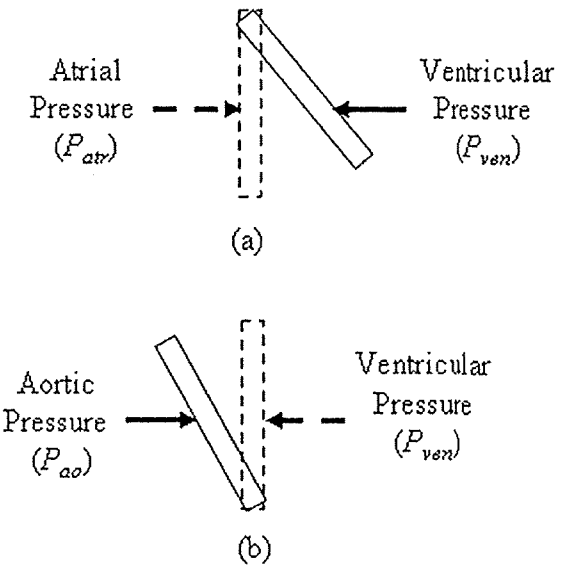

Figure 9. Schematic diagram of pressure causing the valve closure. Inlet valve (A) and outlet valve (B).

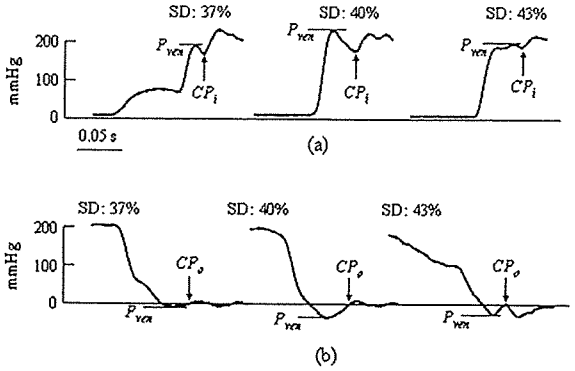

Figure 10. Ventricular pressure just before valve closure. Inlet valve (**A**) and outlet valve (**B**). P_{ven} is peak ventricular pressure just before valve closure, and CP_i and CP_o are the inlet valve and outlet valve closure point, respectively.

and full-ejection condition was higher than under the partial-filling and partial-ejection condition (**Figure 4** and **5**). This suggests that the full-filling and full-ejection condition corresponds to a high valve-closing velocity and a high RMS pressure. However, we could be comparing the systolic duration of 37% with the systolic duration of 40% of all heart rate. Even if the bypass flow decreased to a range of from 7% to 11.2% at the low-systolic duration (**Figure 3**), the RMS pressure of the inlet valve would decrease to the range from 13.4% to 51.2% (**Figure 8**). It is considered that the 10% increase in the stroke volume and the partial-filling and partial-ejection condition (low-systolic duration) caused by the bypass flow, which is decreased by 10% might be an optimal running condition for the VAD size to prevent hemolysis.

In clinical use, the problem of thrombus formation inside the blood pump of the VAD as well as the hemolysis caused by cavitation and high shear stress must be resolved. Our study was restricted to the cavitation intensity of the running condition for our PVAD and thus did not address flow visualization

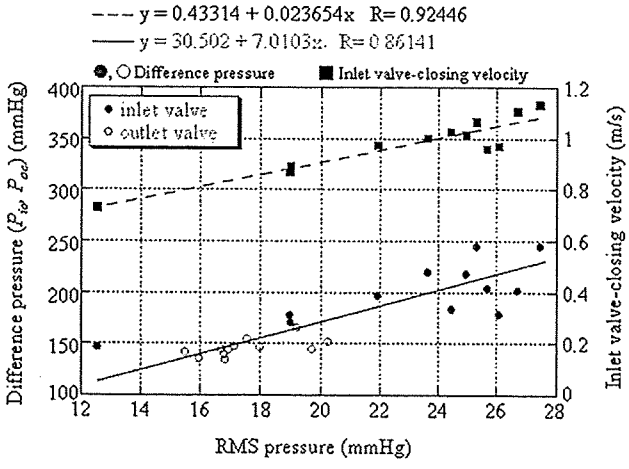

Figure 11. Pressure causing the inlet and the outlet valve closure and inlet valve-closing velocity at various of the RMS pressure. P_{ic} indicates the positive peak ventricular pressure just before inlet valve closure subtracted from the atrial pressure. P_{oc} indicates that the aortic pressure is subtracted from the negative peak ventricular pressure just before outlet valve closure.

inside the blood pump. The full-filling and full-ejection condition was the best condition for blood pump efficiency and washout effect of the inside of the blood pump. Conversely, in the partial-filling and partial-ejection condition, it is possible to decrease the bypass flow and thrombus formation inside the blood pump. As a next step, we will investigate the flow visualization inside the blood pump for our PVAD using a model VAD made of acrylic resin, which has the same geometry as our PVAD.

Conclusion

In this study, we investigated the possibility of cavitation occurrence at the inlet and outlet valve in the PVAD in *in vitro* testing. The RMS pressure of the inlet valve was higher than that of the outlet valve. Even if the RMS pressure of the outlet valve was less than that of the inlet valve, cavitation occurs. During partial-filling and partial-ejection of the blood pump, the PVAD has a small RMS pressure. This means that a partial-filling and partial-ejection condition is considered best for preventing the hemolysis caused by the cavitation phenomenon and the damage to the valve surface in our PVAD system.

Acknowledgment

Supported by the Program for the Promotion of Fundamental Studies in Health Science of the National Institute of Biomedical Innovation (NIBIO) and by a Grant-in-Aid for Scientific Research from the Japan Society for the Promotion of Science (JSPS).

References

1. Knapp RT, Daily JW, Hammitt FG: *Cavitation.* Iowa City, IA, Institute of Hydraulic Research, University of Iowa, 1979.
2. Kornberg A, Wildhirt SM, Schulze C, Kreuzer E: Leaflet escape in Omnicarbon monoleaflet valve. *Eur J Cardiothorac Surg* 15: 867–869, 1999.
3. Klepetko W, Moritz A, Mlczoch J, *et al*: Leaflet fracture in Edward-Duromedics bileaflet valves. *J Thorac Cardiovasc Surg* 97: 90–94, 1989.
4. Johansen P: Mechanical heart valve cavitation. *Expert Rev Med Devices* 1: 95–104, 2004.
5. Lee HS, Tatsumi E, Taenaka Y: Estimation of mechanical heart valve cavitation in a pneumatic ventricular assist device. *J Artif Organs* 10: 181–185, 2007.
6. Lee HS, Taenaka Y: Hydrodynamic characteristics of the Edwards MIRA bileaflet valve in a pneumatic ventricular assist device. *ASAIO J* 53: 397–402, 2007.
7. Rambod E, Beizai M, Sahn DJ, Gharib M: Role of vortices in growth of microbubbles at mitral mechanical heart valve closure. *Ann Biomed Eng* 35: 1131–1145, 2007.
8. Sohn K, Manning KB, Fontaine AA, *et al*: Acoustic and visual characteristic of cavitation induced by mechanical heart valves. *J Heart Valve Dis* 14: 551–558, 2005.
9. He Z, Xi B, Zhu K, Hwang NHC: Mechanisms of mechanical heart valve cavitation: Investigation using a tilting disk valve model. *J Heart Valve Dis* 10: 666–674, 2001.
10. Zapanta C, Stinebring DR, Deutsch S, *et al*: A comparision of the cavitation potential of prosthetic heart valves based on valve closing dynamics. *J Heart Valve Dis* 7: 655–667, 1998.
11. Lee HS, Tatsumi E, Taenaka Y: Effect of systolic duration on mechanical heart valve cavitation in a pneumatic ventricular assist device: Using a monoleaflet valve. *ASAIO J* 54: 25–30, 2008.
12. Lee HS, Taenaka Y: Characteristics of mechanical heart valve cavitation in a pneumatic ventricular assist device. *Artif Organs* 32: 453–460, 2008.
13. Lukic B, Zapanta CM, Griffith KA, Weiss WJ: Effect of the diastolic

and systolic duration on valve cavitation in a pediatric pulsatile ventricular assist device. *ASAIO J* 51: 546–550, 2005.
14. Akagawa E, Lee HS, Tatsumi E, *et al*: Effects of mechanical valve orifice direction on flow pattern in a ventricular assist device, *J Artif Organs* 10: 85–91, 2007.
15. Donovan FM Jr: Design of a hydraulic analog of the circulatory system for evaluating artificial hearts. *Biomater Med Devices Artif Organs* 3: 439–449, 1975.
16. Graf T, Reul H, Detlefs C, *et al*: Causes and formation of cavitation in mechanical heart valve. *J Heart Valve Dis* 3: S49–S64, 1994.
17. Kleine P, Perthel M, Hasenkam JM, *et al*: High-intensity signals (HITS) as a parameter for optimum orientation of mechanical aortic valves. *Thorac Cardiov Surg* 48: 360–363, 2000.
18. Potthast K, Erdönmen G, Schnelke C, *et al*: Origin and appearance of HITS induced by prosthetic heart valves: An in vitro study. *Int J Artif Organs* 23: 441–445, 2000.
19. Wu C, Liu JS, Hwang NHC, Lin YKM: Statistical correlation between transient pressure drop and cavitation at closure of a mechanical heart valve. *ASAIO J* 51: 11–16, 2005.
20. Biancucci BA, Deutsch S, Geselowitz DB, Tarbell JM: In vitro studies of gas bubble formation by mechanical heart valves. *J Heart Valve Dis* 8: 186–196, 1999.
21. Wu C, Herman BA, Retta SM, *et al*: On the closing sounds of a mechanical heart valve. *Ann Biomed Eng* 33:743–750, 2005.
22. Herbertson LH, Reddy V, Manning KB, *et al*: Wavelet transforms in the analysis of mechanical heart valve cavitation. *J Biomech Eng* 128: 217–222, 2006.
23. Lee CS, Chandran KB, Chen LD: Cavitation dynamics of mechanical heart valve prostheses. *Artif Organs* 18: 758–767, 1994.
24. Shu MCS, Leuer LH, Armitage TL, *et al*: In vitro observations of mechanical heart valve cavitation. *J Heart Valve Dis* 3: S85–S93, 1994.
25. Lee HS, Taenaka Y, Kitamura S: Estimation of mechanical heart valve cavitation in an electro-hydraulic total artificial heart. *Artif Organs* 30: 16–23, 2006.
26. Zapanta CM, Stinebring DR, Sneckenberger DS, *et al*: In vivo observation of cavitation on prosthetic heart valves. *ASAIO J* 42: M550–M555, 1996.
27. Garrison LA, Lamson TC, Deutsch S, *et al*: An in-vitro investigation of prosthetic heart valve cavitation in blood. *J Heart Valve Dis* 3: S8–S24, 1994.

Am J Physiol Heart Circ Physiol 296: H1117–H1124, 2009.
First published February 6, 2009; doi:10.1152/ajpheart.01120.2008.

Mechanical work and energetic analysis of eccentric cardiac remodeling in a volume overload heart failure in rats

Yoshiaki Takewa,[1,2,3,4] Elie R. Chemaly,[1,4] Miyako Takaki,[2] Li Fan Liang,[1,4] Hongwei Jin,[1,4] Ioannis Karakikes,[1] Charlotte Morel,[1] Yoshiyuki Taenaka,[3] Eisuke Tatsumi,[3] and Roger J. Hajjar[1,4]

[1]Cardiovascular Research Center, Mount Sinai School of Medicine, New York, New York; [2]Department of Physiology II, Nara Medical University School of Medicine, Nara; and [3]Department of Artificial Organs, National Cardiovascular Center Research Institute, Osaka, Japan; and [4]Cardiovascular Research Center, Massachusetts General Hospital, Harvard Medical School, Boston, Massachusetts

Submitted 24 October 2008; accepted in final form 3 February 2009

Takewa Y, Chemaly ER, Takaki M, Liang LF, Jin H, Karakikes I, Morel C, Taenaka Y, Tatsumi E, Hajjar RJ. Mechanical work and energetic analysis of eccentric cardiac remodeling in a volume overload heart failure in rats. Am J Physiol Heart Circ Physiol 296: H1117–H1124, 2009. First published February 6, 2009; doi:10.1152/ajpheart.01120.2008.—Eccentric cardiac remodeling seen in dilated cardiomyopathy or regurgitant valvular disease is a well-known process of heart failure progression, but its mechanoenergetic profile has not been yet established. We made a volume overload (VO) heart failure model in rats and for the first time investigated left ventricular (LV) mechanical work and energetics in cross-circulated whole heart preparations. Laparotomy was performed in 14 Wistar male rats, and abdominal aortic-inferior vena caval shunt was created in seven rats (VO group). Another seven rats underwent a sham operation without functional shunt (Sham group). LV dimensions changes were followed with weekly transthoracic echocardiography. Three months after surgery, we measured LV pressure and volume and myocardial O_2 consumption in isolated heart cross circulation. LV internal dimensions in both systolic and diastolic phases were significantly increased in the VO group versus the Sham group (P 0.05). LV pressure was markedly decreased in the VO group versus in the Sham group (P 0.05). LV end-systolic pressure-volume relation shifted downward, and myocardial O_2 consumption related to Ca^2 handling significantly decreased. The contractile response to Ca^2 infusion was attenuated. Nevertheless, the increase in Ca^2 handling-related O_2 consumption per unit change in LV contractility in the VO group was significantly higher than that in the Sham group (P 0.05). The levels of sarco(endo)plasmic reticulum Ca^2 -ATPase 2a protein were reduced in the VO group (P 0.01). In conclusion, VO failing rat hearts had a character of marked contractile dysfunction accompanied with less efficient energy utilization in the Ca^2 handling processes. These results suggest that restoring Ca^2 handling in excitation-contraction coupling would improve the contractility of the myocardium after eccentric cardiac remodeling.

eccentric left ventricular hypertrophy; myocardial oxygen consumption; Ca^2 handling; sarco(endo)plasmic reticulum Ca^2 -ATPase 2a; cross circulation; aortocaval shunt

HEART FAILURE IS A MAJOR CAUSE of mortality and morbidity. It is due to various diseases such as hypertension, ischemic heart disease, valvular heart disease, congenital heart disease, cardiomyopathy, myocarditis, and others. The heart is subject to excessive and/or long-term overload, which induces myocardial hypertrophy. Hypertrophy initially compensates cardiac function but finally leads to heart failure. The process of hypertrophy and heart failure progression is divided into two mechanisms, depending on the type of overload: pressure overloading (PO) and volume overloading (VO). PO induces concentric hypertrophy to normalize wall stress from the increase in pressure placed on cardiomyocytes. Concentric remodeling of the left ventricle (LV) is characterized by an increase in ventricular wall thickness due to vertical growing of cardiomyocytes, which is caused by the parallel addition of sarcomeres (8).

Conversely, VO promotes eccentric hypertrophy to compensate for excess blood volume in the LV chamber. Eccentric remodeling of the LV is characterized by a relatively small increase in wall thickness and longitudinal growing of cardiomyocytes.

Morphological analyses, functional studies using echocardiography (4), and molecular studies (10) have been conducted on both PO and VO rat hearts. However, the cardiac mechanoenergetics studies have not yet been well conducted. We have established a method to analyze specifically the LV mechanical work and energetics in an excised, blood-perfused whole heart preparation with a cross-circulation method (7, 14, 17, 19, 20, 24) and analyzed LV mechanoenergetics in a PO heart failure model.

In the present study, we focused on the investigation of the mechanical work and energetics in a VO heart failure model with an arteriovenous (AV) shunt in rats.

MATERIALS AND METHODS

Animals

All animal experiments were performed with the approval of the Animal Care Committee of the Massachusetts General Hospital and the Mount Sinai School of Medicine and in accordance with the National Institutes of Health Guide for the Care and Use of Laboratory Animals. Fourteen male Wistar rats (Charles River, MA) weighing 300–350 g were randomized into two groups: 1) rats subjected to abdominal aortocaval shunt procedures as described previously (VO rats, n 7) (22) and 2) Sham-operated rats (Sham rats, n 7).

Creation of the Animal Models

VO was induced via the aortocaval shunt method (5, 22). All rats were anesthetized for surgery with intraperitoneal injection of 50 mg/kg pentobarbital sodium. After endotracheal intubation, artificial

Address for reprint requests and other correspondence: R. J. Hajjar, Cardiovascular Research Center, Mount Sinai School of Medicine, One Gustave Levy Place, Box 1030, New York, NY 10029 (e-mail: roger.hajjar@mssm.edu).

The costs of publication of this article were defrayed in part by the payment of page charges. The article must therefore be hereby marked "advertisement" in accordance with 18 U.S.C. Section 1734 solely to indicate this fact.

ventilation was initiated. Heparin (200 units ip) was added to prevent thrombosis during aortic and vena caval occlusion and promote shunt patency. Ventral laparotomy was performed, and the abdominal aorta and inferior vena cava were exposed by blunt dissection between the renal arterial branch and the iliac bifurcation. Both vessels were temporally occluded at both proximal and distal sites of the intended shunt point with a Bulldog clip. An 18-gauge angio-catheter was inserted over a needle into the exposed free wall of the abdominal aorta and advanced through the medial wall into the vena cava to create the shunt. After the needle and the angio-catheter were withdrawn, the ventral aortic puncture site was sealed with a drop of cyanoacrylate (Krazy Glue; Elmer's Product Canada, Toronto, Ontario, Canada) to prevent or stop bleeding from the aortic puncture site. Successful shunt could be confirmed by seeing the mixing of oxygenated blood into the vena cava from the abdominal aorta. Sham-operated animals served as controls and were subjected to the same surgeries but had no functional shunt.

Echocardiography

Cardiac function after shunt creation was monitored weekly with transthoracic echocardiography (M mode and pulse wave Doppler) using a Vivid 7 ultrasound system (GE Healthcare, Waukesha, WI) equipped with a 14-MHz transducer under sedation with a low dose (25 mg/kg ip) of pentobarbital sodium. An M-mode pacing of the LV was obtained from the parasternal short-axis view at the level of the papillary muscles. M-mode recordings were then analyzed at a sweep speed of 150 mm/s with the axis of the probe aligned with the middle of the ventricle. The following parameters were measured and calculated using the leading edge method described by the American Society of Echocardiography (4, 12): LV internal dimensions (LVID) at both diastole and systole (LVIDd and LVIDs, respectively), LV posterior wall dimensions at both diastole and systole, interventricular septal (IVS) dimensions at both diastole (IVSd) and systole, heart rate (HR), percentage of LV fractional shortening, LV ejection fraction (EF), and cardiac output.

LV Mechanical and Energetic Studies

Surgical preparations. LV mechanical and energetic studies were performed 3 mo after the creation of aortocaval shunt on the excised cross-circulated rat heart preparations, as reported previously (13). In each experiment, one VO or Sham rat and two retired breeder male crj:Wistar rats weighing 450–650 g were anesthetized with pentobarbital sodium (50 mg/kg ip), intubated, and ventilated. The study rat (VO or Sham) was used as heart donor, and the other two were used as blood supplier and metabolic supporter rats, respectively. All rats were heparinized (1,000 units intravascular). The beating donor heart was excised without an interruption of coronary perfusion and supported by cross circulation with the other metabolic supporter rat as previously reported in detail (7, 14, 17, 19, 24). The coronary arterial oxygenated blood of the donor heart was supplied from the common carotid arteries of the supporter rat using arterial cross-circulation tubing and a cannula inserted into the brachiocephalic artery of the donor heart. The coronary venous blood of the donor heart was collected from a cannula inserted into the right ventricle (RV) via the superior vena cava and the right atrium and returned to the right external jugular vein of the supporter rat using venous cross-circulation tubing and a cannula. The excised heart was maintained at 37°C by a heater. A thin latex balloon (balloon material volume, 0.08 or 0.10 ml) was inserted from the left atrial appendage into the LV and primed with water. The maximum unstretched volume of the used balloon was large enough to exceed measured end-diastolic volume in both VO and Sham rat hearts. The balloon was connected to a 0.5-ml precision glass syringe with fine scales (minimum scale, 0.005 ml) to allow changing LV volume (LVV) in 0.025-ml steps and also connected to a pressure transducer for measuring LV pressure (LVP) measurement. LVV was increased in steps up to an end-diastolic pressure (EDP) of around 10 mmHg in the control volume run. Systolic unstressed volume (V_0) was determined by filling the balloon to the level where peak isovolumic pressure and hence pressure-volume area (PVA; see Data Analysis) were zero. The sum of intraballoon water volume and balloon material volume was used as an initial estimate of V_0. V_0 normalized by LV mass to 1 g was then finally determined as the volume-axis intercept of the best-fit end-systolic pressure (ESP)-volume relation (ESPVR). We obtained the best-fit ESPVR with an equation (ESP A{1 exp[B(V V_0)]}; A and B are parameters) by means of the least-squares method (DeltaGraph, DeltaPoint; Monterey, CA) on a personal computer (14, 17, 19, 24). We also obtained the best-fit EDP-volume relation (EDPVR) with an equation (EDP A {exp[B (V V_0)] 1}; A and B are parameters). Correlation coefficients of the best-fit ESPVRs were higher than 0.98 (Table 1).

The HR was constantly maintained by electrical pacing of the right atrium, and the pacing rate was adjusted around 300 beats/min to avoid causing incomplete relaxation or arrhythmia. The systemic arterial blood pressure of the supporter rat served as the coronary perfusion pressure (90–120 mmHg). Arterial O_2 saturation and O_2 content of the supporter rat were monitored with an oximeter (model IL682 CO-Oxymeter; Instrumentation Laboratory) and maintained within their physiological ranges with ventilation adjustment and supplemental O_2 and sodium bicarbonate.

Calculation of O_2 consumption. Total myocardial O_2 consumption per beat ($\dot{V}O_2$) was obtained as the product of coronary flow and coronary AV O_2 content difference (AVO_2D) divided by the pacing rate (300 beats/min) (14, 17, 19, 24). Total coronary blood flow was continuously measured with an ultrasonic flowmeter (model T206; Transonic System, Ithaca, NY) placed in the middle of the venous drainage tubing from the RV. LV thebesian flow is negligible. The coronary AVO_2D was continuously measured by passing all the arterial and venous cross-circulation blood through the cuvettes of a custom-made AVO_2D analyzer (PWA-200S, Shoe Technica; Chiba, Japan) as previously reported in detail (14, 17, 19, 24).

Calculation of PVA. PVA was defined as the systolic PVA circumscribed by the curvilinear ESPVR, the EDPVR, and the systolic portion of the ventricular pressure-volume trajectory and was obtained by the integration of ESPVR and EDPVR. The areas under the ESPVR and EDPVR were obtained by the integration of the best-fit exponential functions. Based on our previous publications (14, 17, 19, 24), we obtained control ESPVR and determined a midrange LV volume (mLVV) under which contractility changes in response to Ca^2 infusion (16). As the balloon volume generally changed between 0 and 0.10 ml in Sham rats and between 0 and 0.20 ml in VO rats, respectively, we adopted mLVV normalized by LV mass to 1 g at balloon volume of 0.05 ml for Sham LVs and at balloon volume of 0.10 ml for VO LVs. We calculated ESP at mLVV (ESP_{mLVV}) and PVA at mLVV (PVA_{mLVV}) to assess LV mechanical work and energetics in the two groups.

As shown previously (14, 17, 19, 24), the $\dot{V}O_2$-PVA relationship was linear in the rat LV. Its slope represents the O_2 cost of PVA, and

Table 1. Variables of bodies, hearts, and lungs

	Sham		VO		P
Body weight, g	609	81	609	66	0.823
LV weight, g	1.05	0.15	1.41	0.21	0.016*
RV weight, g	0.23	0.04	0.38	0.07	0.006*
LV RV weight, g	1.28	0.18	1.79	0.26	0.008*
LV weight/body weight, %	0.17	0.02	0.23	0.02	0.007*
RV weight/body weight, %	0.03	0.01	0.06	0.01	0.005*
LV RV weight/body weight, %	0.21	0.02	0.29	0.03	0.004*
Lung weight, g	1.97	0.47	2.26	0.48	0.319

Values are means SD; n 7 Sham rats and 7 volume overload (VO) rats. LV, left ventricle; RV, right ventricle; P, value of probability. *P 0.05 vs. Sham.

its $\dot{V}O_2$ intercept represents the PVA-independent $\dot{V}O_2$. The PVA-independent $\dot{V}O_2$ is composed of $\dot{V}O_2$ in excitation-contraction (E-C) coupling (18) and basal metabolism (11, 17). The RV was kept collapsed (and therefore unloaded) by continuous hydrostatic drainage of the coronary venous return so that the RV PVA and hence PVA-dependent $\dot{V}O_2$ were assumed to be negligible (19, 20). The RV component of total $\dot{V}O_2$, which is considered constant irrespective of LV volume, was calculated by multiplying biventricular $\dot{V}O_2$ under unloaded LV volume with the ratio of the RV weight divided by the sum of the RV and LV weight. The RV PVA-independent $\dot{V}O_2$ (14, 17, 19, 24) was subtracted from the total $\dot{V}O_2$ to yield LV $\dot{V}O_2$ expressed as $\dot{V}O_2$. The LV (including the septum) and the RV were weighed at the end of the experiment for normalization of LVV.

Experimental protocol. LVP, LV $\dot{V}O_2$, and systolic PVA data were obtained at more than five different LV volumes from 0 to 0.2 ml of intraballoon volume in 0.025-ml increments, without inotropic interventions [control volume-loading run (vol-run)]. After the vol-run, the Ca^2 inotropic run (Ca^2 ino-run) was performed at an mLVV by intracoronary infusion of 1% $CaCl_2$ solution. The infusion rate of $CaCl_2$ solution was increased stepwise from 0 to 6 ml/h. Steady-state $\dot{V}O_2$ was reached 2 to 3 min after change of LV volume and 4 min after change of infusion rate. Finally, cardiac arrest was induced by intracoronary infusion of 1 M KCl (12 ml/h) to obtain O_2 consumption for basal metabolism. At each steady state, data were sampled at 500 Hz for 2 s simultaneously, and the sampling was usually repeated three times at 0.5- to 1-min intervals.

Data Analysis

$\dot{V}O_2$ for Ca^2 handling during the Ca^2 ino-run. In previous mechanoenergetic studies in excised rat hearts (14, 17, 19, 24), a linear $\dot{V}O_2$-PVA relation obtained during Ca^2 infusion (Ca^2 $\dot{V}O_2$-PVA relation) was shifted upward in parallel with the control $\dot{V}O_2$-PVA relation before Ca^2 infusion. Such parallelism was also observed in VO rat hearts in our preliminary experiments. The $\dot{V}O_2$-intercept (PVA-independent $\dot{V}O_2$) corresponds primarily to the $\dot{V}O_2$ for Ca^2 handling in E-C coupling and for basal metabolism (11, 17, 18). The increased $\dot{V}O_2$ intercept of the Ca^2 $\dot{V}O_2$-PVA relation is attributable to the increased $\dot{V}O_2$ for enhanced Ca^2 handling due to the unchanged $\dot{V}O_2$ for basal metabolism (17). Thus, at increasing levels of inotropy, the intercept of the $\dot{V}O_2$-PVA relationship increases, but the slope remains unchanged. Based on this parallelism, the lines of $\dot{V}O_2$-PVA linear relationships at different rates of Ca^2 infusion at an mLVV were drawn in parallel to the control $\dot{V}O_2$-PVA relation line, as described previously (14, 17, 19, 24).

During the Ca^2 ino-run at an mLVV, ESPVR curves at different infusion rates were obtained as best-fit exponential function curves. We calculated PVA_{mLVV} during Ca^2 infusion on a personal computer (14, 17, 19, 24). We then obtained the two composite $\dot{V}O_2$-PVA_{mLVV} data points. After we drew the lines, including each $\dot{V}O_2$-PVA_{mLVV} data point, in parallel to the control $\dot{V}O_2$-PVA relation, we obtained the $\dot{V}O_2$ intercept at each infusion rate. We subtracted basal metabolic $\dot{V}O_2$ per beat, measured in KCl-arrested hearts, from PVA-independent $\dot{V}O_2$ to obtain $\dot{V}O_2$ for Ca^2 handling in E-C coupling.

LV contractility. Our recently proposed index for LV contractility (i.e., equivalent maximal elastance [eE_{max}]) was calculated from ESP-volume ratio of the specific virtual triangular area, which is energetically equivalent to PVA_{mLVV} as previously described (17, 20).

O_2 cost of LV contractility. The O_2 cost of LV contractility was obtained as the slope of the linear relation between $\dot{V}O_2$ for Ca^2 handling in E-C coupling and eE_{max} at an mLVV during the Ca^2 ino-run. At every infusion rate, there was a corresponding eE_{max} and a corresponding $\dot{V}O_2$ for Ca^2 handling in E-C coupling derived from the $\dot{V}O_2$-PVA intercept (PVA-independent $\dot{V}O_2$). eE_{max} and PVA-independent $\dot{V}O_2$ were also linearly related. The slope of the latter linear relationship, defined as the O_2 cost of LV contractility, quantifies the change in $\dot{V}O_2$ for Ca^2 handling per unit change in LV contractility.

Western blot for sarco(endo)plasmic reticulum Ca^2 -ATPase 2a and sodium-calcium exchanger proteins. LV myocardium from each heart was frozen and stored at 80°C after the mechanoenergetic studies. The frozen hearts were thawed and homogenized. The homogenates were matched for protein concentration, subjected to SDS-PAGE, and transferred to nitrocellulose membranes. For immunoreactions, the blots were incubated with primary antibodies to sarco(endo)plasmic reticulum Ca^2 -ATPase 2a (SERCA2a; Affinity Bioreagents, Golden, CO), sodium-calcium exchanger (NCX)1 [Chemicon (Millipore), Billerica, MA], and GAPDH (Sigma-Aldrich, St. Louis, MO) and then subjected to enhanced chemiluminescence for detection. Both SERCA2a and NCX1 expressions were normalized to GAPDH expression.

Statistical analysis. Values are means SD. Comparison of paired and unpaired individual values was performed by the paired and unpaired t-test, respectively. A value of P 0.05 was considered statistically significant. All data are expressed as the means SD.

RESULTS

Echocardiography

Typical M-mode echocardiograms in both VO and sham rats 10 wk after operation are displayed in Fig. 1.

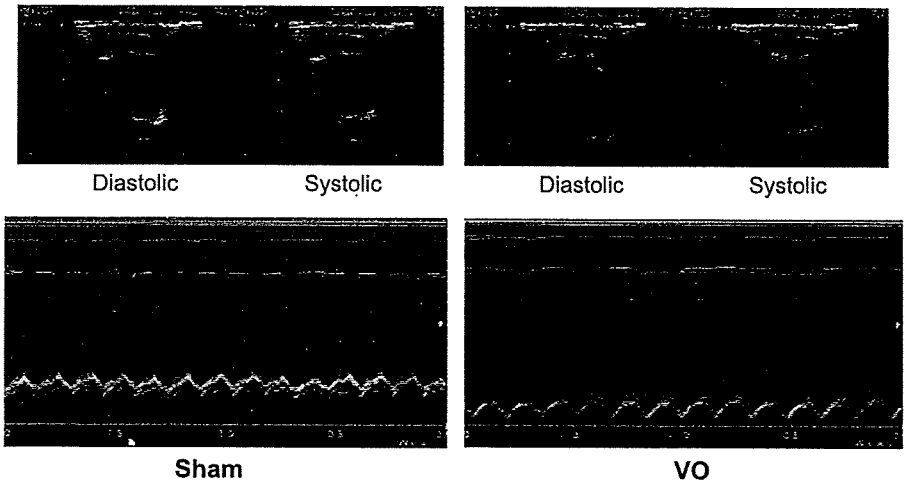

Fig. 1. Representative M-mode echocardiograms in both volume overloading (VO) and Sham rats 10 wk after aortocaval shunt creation. Left ventricular (LV) internal dimensions at both diastole and systole (LVIDd and LVIDs, respectively) were markedly increased in VO rats compared with those in Sham rats.